Important Notice

UNIVERSITY OF CALGARY

Monitoring fluid injection using seismic time-lapse analysis: a Rainbow Lake case study

by

Hannah Ng

A THESIS

SUBMITTED TO THE FACULTY OF GRADUATE STUDIES

IN PARTIAL FULFILMENT OF THE REQUIREMENTS FOR THE

DEGREE OF MASTER OF SCIENCE

DEPARTMENT OF GEOLOGY AND GEOPHYSICS

CALGARY, ALBERTA

JANUARY, 2005

UNIVERSITY OF CALGARY

FACULTY OF GRADUATE STUDIES

The undersigned certify that they have read, and recommend to the Faculty of Graduate Studies for acceptance, a thesis entitled " Monitoring fluid injection using seismic time-lapse analysis: a Rainbow Lake case study" submitted by Hannah Ng in partial fulfilment of the requirements of the degree of Master of Science.

Supervisor, Dr. E.S. Krebes
Department of Geology & Geophysics

Co-Supervisor, Dr. L.R. Bentley
Department of Geology & Geophysics

Dr. G. Margrave
Department of Geology & Geophysics

Dr. M. Pooladi-Darvish
Department of Chemical and Petroleum Engineering

Date

Abstract

The Rainbow B pool, a carbonate reservoir, is undergoing solvent and gas injection to extract the remaining oil. Although not commonly done because the expected seismic changes are small, time-lapse or 4D processing and interpretation are applied to two sets of 3D data to detect the locations of the injected fluids. The presence of gas and solvent were best interpreted with the time-delay results, as opposed to the amplitude change results. Fluid related changes were detected in vuggy or low pore aspect ratio porosity zones but changes were not detectable in zones with intergranular porosity. Because the reservoir is extremely heterogeneous and the pore geometry greatly affects the results, this study could detect changes in some but not all locations of the reservoir. This study also showed that the Gassmann equation underpredicts velocity changes in this reservoir. Also, the seismic time-delay results matched the engineering simulation data fairly well.

Acknowledgements

First of all, I would like to thank Larry Mewhort at Husky Energy Inc. for introducing me to this project. I appreciate all his guidance and useful suggestions. Other appreciated help came from Ken Hedlin, a geophysicist, Larry Carr, an engineer, and Andre Laflamme, a geologist. Husky Energy provided the data and in particular, the Husky B Pool Asset Team Engineers and Geologists provided the reservoir simulation results. Keith Hirsche and Francis Ma from Hampson-Russell Ltd. Partnership were also helpful. I would also like to thank the CREWES sponsors, staff and students. John Zhang and Ying Zou, my fellow colleagues, provided some useful feedback. Also, I am grateful for the help of my supervisors, Edward Krebes and Larry Bentley. Finally, I thank my husband for his unconditional love and support.

Table of Contents

List of Tables

List of Figures and Illustrations

List of Symbols, Abbreviations and Nomenclature

V_P	compressional or P-wave velocity
V_S	shear or S-wave velocity
K	bulk modulus
μ	shear modulus
ρ	density
ρ_w	water density
ρ_o	oil density
ρ_g	gas density
ρ_{sol}	solvent density
K_w	water modulus
K_o	oil modulus
K_g	gas modulus
K_{sol}	solvent modulus
K_{sat}	modulus of a fluid saturated rock
K_{dry}	modulus of a dry rock
K_{fl}	modulus of the fluids
K_s	modulus of the solid minerals making up the rock
S_w	water saturation
S_o	oil saturation

S_g	gas saturation
S_{sol}	solvent saturation
φ	porosity
σ	net or effective pressure
S	overburden pressure
p	pore pressure
ms	milliseconds
KPa	kiloPascal
MPa	megaPascal
GPa	gigaPascal
rms	root mean square
mD	milliDarcy
Hz	Hertz
API	American Petroleum Institute
°C	degrees Celsius
m	metres
OOIP	original oil in place
GOR	gas oil ratio

Chapter One: INTRODUCTION

1.1 What is time-lapse seismic?

Time-lapse seismic or 4D seismic refers to a seismic survey repeated in the same area after a period of time in an effort to image changes that could have occurred in a reservoir. Four-D refers to the fourth dimension of a 3D seismic survey, where the fourth dimension is time. The time-lapse method is useful in that reservoir changes *in between* wells can be detected. Time-lapse analysis is also used to improve production by identifying locations of bypassed oil. Two or more seismic surveys, acquired at different times but in the same area, are compared to one another to determine whether there are any seismic attribute changes such as travel time differences, reflection amplitude differences or seismic velocity differences. The differences indicate changes in the reservoir properties.

Time-lapse seismic is analogous to photographing a person at different years of his/her life. Then, the photographs are analyzed to see what changes have occurred. Similarly, we take photographs or acquire seismic surveys of the reservoir at different times. Then, we analyze the seismic data to see what changes have occurred. In our photography analogy, the photos need to be made similar in terms of size, colour and resolution before they can be compared to one another. The seismic surveys also need to be made similar to one another in terms of frequency, time and amplitude before they can be compared. The process of matching the seismic surveys is referred to as time-lapse processing. Time-lapse processing removes differences between the seismic surveys that are not due to production changes in the reservoir.

A "zero-time repeatability test" is a test that is used to gauge how well the surveys are matched to each other after acquisition. Basically, two seismic surveys are acquired one after the other without any passing of time and so there should be no production changes. Then the surveys are subtracted one from the other and if the differences between the surveys are close to zero, then the surveys are well matched.

1.2 Time-lapse analysis case studies

Within the past decade, there have been over 100 case studies analyzed using the time-lapse method (Lumley, 2001a). Also, 50% of the seismic surveys in the North Sea are being acquired for time-lapse purposes (Jack, 1998). Time-lapse analysis is becoming popular as many reservoirs are being depleted and tertiary recovery methods are applied. This is because time-lapse analysis helps detect remaining oil and gas in a reservoir. Primary recovery consists of using the natural drives of the reservoir to deplete oil or gas and is usually the first method used to produce hydrocarbons. Secondary recovery consists of waterflooding a reservoir and tertiary recovery or enhanced oil recovery (EOR) is usually the final method of depleting a reservoir. This may consist of flooding a reservoir with solvent, CO_2, or using thermal methods to deplete oil. The time-lapse method is used more often in the tertiary recovery phase than in the primary or secondary recovery phase. This is because the fluid modulus changes or the fluid compressibility changes are greater and thus the changes are easier to detect in seismic data. For example, waterflooding a reservoir is a secondary recovery phase and time-lapse analysis is not commonly done in this phase. It consists of injecting water to displace oil. The fluid modulus difference between water and oil is very small and thus, seismic changes are subtle and may or may not be detectable on data, although as seismic

data and techniques improve, there are case studies where time-lapse analysis is done during primary and secondary recovery. The case studies discussed below are for the tertiary recovery case.

The time-lapse method was first tested in the rock physics laboratory using heavy-oil saturated core samples (Wang and Nur, 1990). When the cores were heated, velocity changes as high as 40-50% were detected. The study suggested that these velocity changes could also be detected in seismic data.

One of the earliest well-known time-lapse case studies is the Holt fireflood of Texas, United States (Greaves and Fulp, 1987). The sand reservoir was ignited in order to move oil out of the reservoir. Seismic surveys were acquired prior to heating and also during different phases of heating. The seismic surveys during heating showed bright spots in the locations where oil was converted to gas. Although this method of tertiary recovery is not recommended because of safety and economic issues, the time-lapse method clearly showed the locations of gas.

A steamflood case study using the time-lapse method is the Duri Steamflood of Indonesia (Jenkins et al., 1997; Waite and Sigit, 1997). The Miocene sandstone has high porosity (34%) and high permeability (150 mD). Velocity pulldown or time-delay was detected at the location of the steam front. This steamflood is one of the world's largest with 900 injection wells. The time-lapse method showed good results and thus more surveys in this area were acquired for time-lapse purposes.

A carbonate case study using the time-lapse method is the Weyburn field of Saskatchewan, Canada (Brown et al., 2002; Davis, et al., 2003; Li, 2003; Terrell et al., 2002). The Weyburn program is the largest horizontal injection program in the world

(Terrell et al., 2002), with 1.4 billion barrels of oil in place. The low porosity but high permeability carbonate Vuggy zone is overlain by the high porosity and low permeability carbonate Marly zone. A time-lapse program was set up to detect any bypassed oil in the Marly zone. Two 9-C land surveys were acquired: one prior to flooding in 2001 and one after flooding in 2002. The reservoir was flooded with miscible CO_2 . Parts of the reservoir flooded with CO_2 will have lower impedance than parts with only oil in the pore space. Time-differences were not analyzed because the reservoir is too thin. But, the amplitude differences showed CO_2 fingering and also, the vertical movement of CO_2 was discovered along the high permeability zones (Terrell et al., 2002; Brown et al., 2002).

Another carbonate case study is for the Vacuum field of New Mexico, United States (Talley et al., 1998). CO_2 was flooded into the San Andres carbonates to extract the oil. 3C-3D surveys were used to determine whether the CO_2 was leaking through a fault zone. They found that CO_2 was best detected with shear wave data.

We have discussed various methods of tertiary recovery such as fireflood recovery, steam recovery, and CO_2 recovery. In the future, there may be instrumented oil fields where the sources and the receivers in a field are permanent. Any reservoir changes can be imaged immediately so that the injection and production wells can react to the changes on site (Lumley, 2001b).

1.3 Factors that determine whether time-lapse analysis is feasible

The above case studies describe time-lapse projects that were successfully applied. Prior to acquiring expensive seismic data for a time-lapse project, oil and gas companies have to determine whether or not the time-lapse project will be feasible or not. Sometimes, companies purposely set out to shoot seismic data for time-lapse analysis.

The first survey is usually acquired before tertiary production and may be called the Base survey while later surveys are referred to as the Monitor surveys. Other times, companies already have legacy data (pre-existing data) and may set out to acquire the Monitor seismic data. There are various factors that determine whether a time-lapse project will be feasible or not. Described below are various authors' viewpoints on how to assess how risky a time-lapse project is.

Jack (1998) suggested that there is a low chance of success of a time-lapse project in cases where the porosity is less than 15%, in carbonate reservoirs, in reservoirs deeper than 3 km, and in consolidated reservoirs.

Lumley et al. (1997) made a detailed worksheet to assess the technical risk of a time-lapse project. Various parameters in a reservoir, such as the moduli and the image quality, are put into a worksheet. A score is calculated and used to determine whether the time-lapse project is feasible or too risky.

Wang (1997) describes four different factors that make a time-lapse project successful. The first is that the bulk modulus and the shear modulus of the rock frame must be low. This applies to unconsolidated rocks, rocks with open fractures, low pore aspect ratio rocks, and rocks under low net pressure.

The next factor is that there should be a contrast in pore fluid compressibility from one survey to the next. For example, gas and water have a big contrast in compressibility. Also, the amount of gas dissolved in oil, referred to as the gas-oil-ratio (GOR), has an effect on the compressibility of oil. Live oils (oils with dissolved gases) or oils with a high GOR are more compressible than dead oils (oils without dissolved

gases). Also, brines with a lower salinity are more compressible than brines with a higher salinity.

The third factor is the type of recovery. Time-lapse seismic changes are easier to detect in steam injection recovery processes than in CO_2 and gas injection recovery processes because an increase in temperature and pressure can significantly affect the physical property of the rock. But, only subtle changes may be seen in the injection of water into a reservoir with dead oil.

The fourth factor is the reservoir character. This includes the depth of the reservoir. Shallow reservoirs are good candidates because they have a weak elastic frame. Also, pressure and temperature are factors that affect whether time-lapse analysis is feasible or not.

1.4 Pore geometry is an important factor

Figure 1 shows a graph of the compressional wave velocity measured for carbonate rocks with different pore types but the same porosity of 22%. The velocity is higher for the moldic porosity type rock than for the interparticle porosity type rock even though the magnitude of the porosity is the same. The pore geometry has a big effect on the velocity (Kuster and Toksöz, 1974). The pore geometry can be characterized by the pore aspect ratio. The pore aspect ratio is defined as the length of the short axis divided by the length of the long axis in a 2D pore space and the ratio is always less than or equal to one (Wang, 2001).

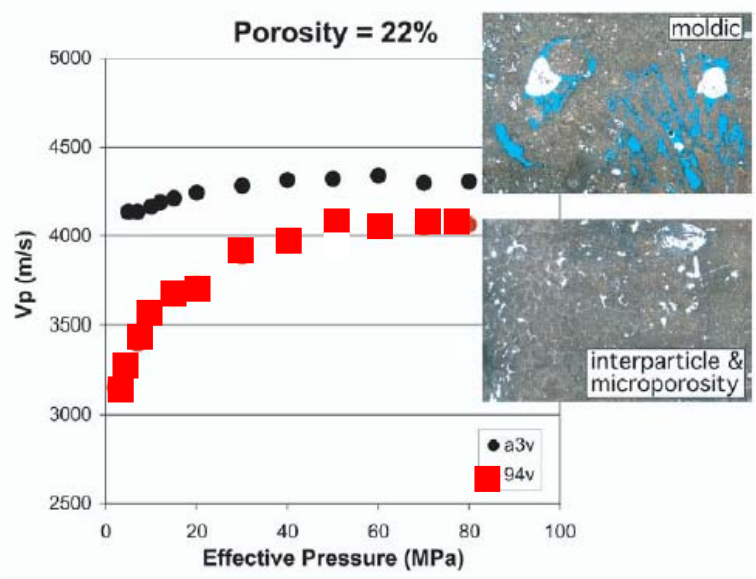

Figure 1. Velocity versus pressure graph. Comparison of carbonate samples with the same porosity of 22% but different pore types. The moldic porosity type rock (a3v) has higher velocity than the interparticle porosity type rock (94v) even though the porosity is the same. (Eberli et al., 2003)

The pore geometry influences the velocity but how does it affect the *velocity change* when a rock is saturated with a different fluid? Hirsche and Hirsche (1998) and Hirsche et al. (1997), along with Western Geophysical and the Alberta Research Counsel, researched the effects of hydrocarbon miscible floods in carbonate reservoirs. They flooded 90 carbonate core samples of different rock types with miscible solvent followed by methane. Figure 2 shows the velocity measured from two carbonate rock samples with different pore types. The rock sample with round high aspect ratio pores did not show any velocity change after fluid was injected but the rock sample with flat low aspect ratio pores (cracks and fractures) showed changes.

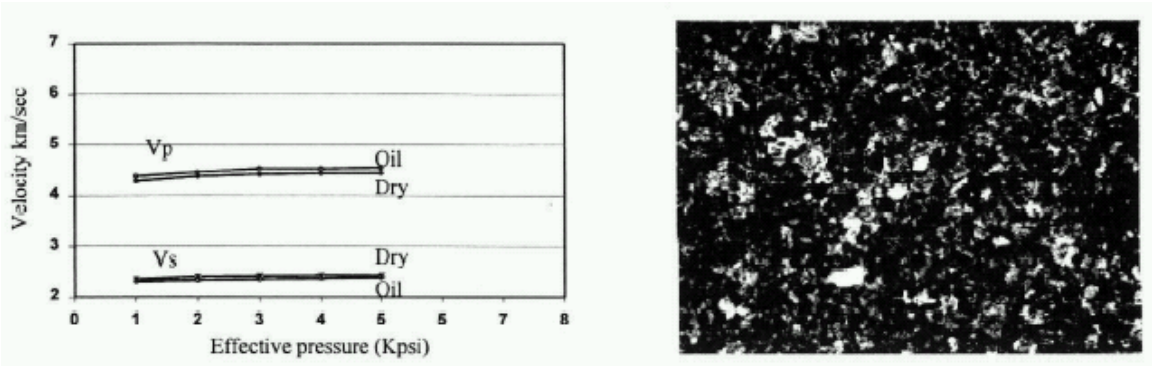

a)

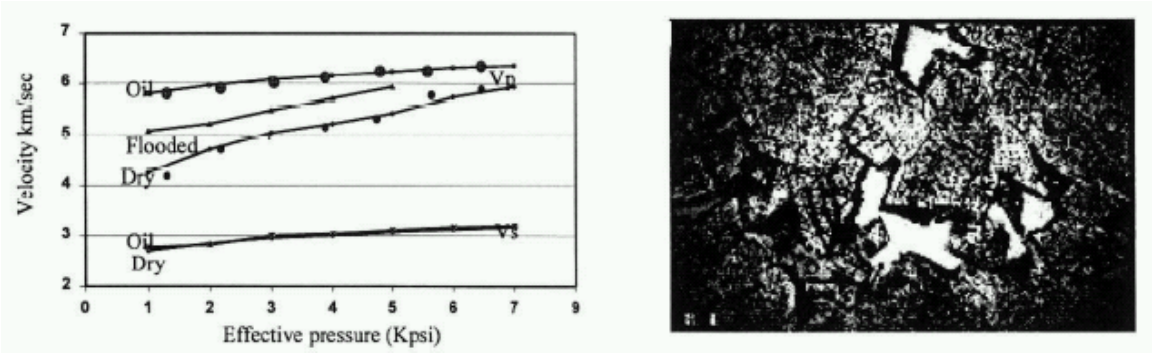

b)

Figure 2. a) Velocity versus pressure graph; corresponding thin section (on right) shows round high aspect ratio pores b) velocity versus pressure graph; corresponding thin section (on right) shows flat low aspect ratio pores (Hirsche et al., 1997)

1.5 The Gassmann equation underpredicts velocity changes

Hirsche and Hirsche (1998) and Hirsche et al. (1997) also applied time-lapse analysis on 2D seismic lines, acquired in 1987 and 1997, for the Rainbow B pool. They discovered that the seismic velocity changes, from pre- to post-tertiary production, are bigger than the calculated velocity changes using the Gassmann equation. Gassmann equation is an equation used to calculate the effects of fluid substitution on the bulk modulus, which is related to the velocity.

The reason for this (Hirsche and Hirsche, 1998) is because one of the Gassmann equation assumptions is violated, that assumption being that the frequency must be low enough so that as the seismic wave propagates through the rock, the pore pressures have enough time to equilibrate. Under normal circumstances, the Gassmann equation will work for the low frequency range found in seismic data. But, because the pore geometry of the Rainbow B pool is mostly vuggy and has a low pore aspect ratio, the frequency range may not be low enough for the pore pressure to equilibrate. The pressure builds and the Gassmann low frequency assumption is violated. Thus, the Gassmann calculated changes are small.

In a real case scenario, the cracks and the vugs weaken the rock frame and make the rock more sensitive to fluid saturation.

1.6 The Rainbow B study

Time-lapse analysis will be applied to the Rainbow B pool. The Rainbow B pool has been producing oil from the carbonate Keg River formation since 1965. Currently, the pool is in the tertiary production phase where miscible gas and solvent are injected into the top of the reservoir in order to produce the remaining oil. A 3D seismic survey was acquired in 1987 and another seismic survey was acquired in 2002, 15 years later. Time-lapse analysis could be used to detect the locations within the reservoir where gas and solvent are believed to be. This could help the engineers determine how well the tertiary production process is working.

1.6.1 Significance of study

An ideal reservoir for time-lapse analysis would be an unconsolidated, highly porous sand reservoir with a high GOR (gas-oil-ratio) that is undergoing steam injection. At a quick overview, time-lapse analysis for the Rainbow B pool does not appear to be feasible. This is because the reservoir is fairly deep at a depth of 1800 m, the porosity is only 8%, and the method of recovery is not steam injection but miscible gas and solvent injection. The high temperature and pressure changes in steam recovery processes cause substantial seismic changes. But, in this study there are negligible temperature and pressure changes. The changes detected are due to fluid changes from gas and solvent to oil.

The Rainbow B pool also does not appear to be feasible for time-lapse analysis because the reservoir is a carbonate reservoir. It is more difficult to detect seismic changes in carbonate reservoirs than in sand reservoirs because the dry bulk modulus of carbonate dominates the rock strength and the low modulus of the fluids and therefore, the high bulk modulus masks the effects of the seismic fluid changes. The significance of this study is that time-lapse analysis is applied to a carbonate pool undergoing gas and solvent injection even though it is not commonly done for carbonates. There are very few time-lapse case studies involving carbonate reservoirs, mainly because the seismic velocity changes are thought to be too subtle to be detected.

Fortunately, the pore geometry of the Rainbow B pool is the factor that causes the seismic differences to be detectable and thus the factor that makes this study feasible for time-lapse analysis. The Rainbow B pool has mainly vug-type porosity. Also, most

areas of the reservoir that are vuggy also have flat pores and cracks, which allow fluid changes to be more detectable on seismic data.

Another reason that time-lapse analysis should be feasible for this pool is that Hirsche and Hirsche (1998) have already shown that time-lapse analysis works using 2D Rainbow B seismic lines. This study will examine the rest of the reservoir using 3D seismic data. Hirsche and Hirsche (1998) have also shown that the velocity changes are greater than the Gassmann equation predicted.

1.6.2 Objective and technique of study

We know where the injection wells are in the reservoir but we don't know where the injected fluids have moved to within the reservoir. The objective of this study is to determine the locations of the injected gas and solvent within the Rainbow B reservoir using time-lapse analysis.

The technique used in this study is to first match the two sets of seismic surveys: the 1987 Base survey and the 2002 Monitor survey. Matching the two surveys is referred to as time-lapse processing. Then, the surveys can be subtracted or crosscorrelated to determine any differences. The seismic changes interpreted are time differences, reflection amplitude differences and impedance differences. These differences are dependent on the seismic velocity and the density of both the fluids and the rock in the reservoir. The differences between the two surveys show the locations of any production related changes in the reservoir. This will help determine whether there are areas of by-passed oil or whether there are any inefficiencies of the production process. Finally, the

seismic results are interpreted with respect to the geological data and the reservoir engineering data.

1.7 Data and software

1.7.1 Data

The main data used for this research project are the seismic data and the reservoir engineering data. The data are courtesy of Husky Energy Inc. The seismic data consist of two sets of 3D seismic surveys acquired 15 years apart. The first survey was acquired in 1987 while the second survey was acquired in 2002. Only V_P seismic data are available and not V_S. Also, sonic logs with V_P data are available and not V_S. The reservoir engineering data consist of the reservoir simulation results. Geological data, such as core and well logs, were also observed and analyzed. Log data were only available prior to flooding.

1.7.2 Software

1.7.2.1 Geophysics software

The seismic software mainly used for this research project is from Hampson-Russell Ltd. Partnership. PRO4D is the software used for 4D seismic analysis. Other programs used include HRS STRATA, which is an inversion program, and HRS ISMAP, which is a mapping program.

1.7.2.2 Engineering software

The reservoir engineering software used is from the Computer Modelling Group Ltd. (CMG). The reservoir engineers use this program to do reservoir simulation and

history matching. This simulation can be used to determine the reservoir capacities, predict the reservoir production and determine how long it will take for the hydrocarbons to be depleted. A specific program within CMG, called Results3D, displays the results of the simulation in map view and in cross-sectional view in order for the reservoir to be easily visualized. The Husky B Pool Asset Team Engineers and Geologists built the reservoir model. The Rainbow B pool was split into different sized grid blocks in the reservoir simulation. There are 25 columns, 60 rows, and 41 layers, for a total of 61, 500 grid blocks. The porosity and the permeability data were put into the reservoir simulation while the pressure and the fluid saturation data were extracted from the simulation. These data will be used in this study.

1.7.2.3 Other software

Other software used includes IHS Energy's Accumap software and Mathworks' MATLAB 6.0 computing language, and Microsoft's Excel spreadsheet.

1.8 Outline of thesis

Chapter two discusses the rock physics. Rock physics is important because it provides the link between the seismic data and the rock data. Chapter three discusses the geological background, the reservoir engineering background, and the seismic background of the Rainbow B pool. Chapter four discusses the time-lapse processing steps that I applied prior to comparing the surveys. Chapter five shows the seismic time-lapse results. The results are shown as a time-delay map, an amplitude change map and an impedance change map. Chapter six discusses the comparison between the time-delay maps versus the geological map and the engineering map.

Chapter Two: ROCK PHYSICS THEORY

2.1 Introduction

Rock physics is an important aspect of time-lapse analysis because rock and fluid properties can be linked to seismic properties. One of the most important equations in time-lapse analysis is the Gassmann (1951) equation, which is an equation used to predict the change in seismic parameters with respect to fluid changes. In this study, miscible gas and solvent are displacing oil. Using the Gassmann equation, we can determine what kind of seismic changes can be expected from this type of recovery. Then the theoretical results using the Gassmann equation can be compared to the actual seismic time-lapse results. The main factors that affect the time-lapse results are pressure, temperature, fluid type and porosity.

2.2 Rock physics link to seismic

Rock physics is used to describe the relationship between the rock properties and the seismic properties. A rock may be described in terms of its elastic parameters: shear modulus (μ) is the resistance to shear, and bulk modulus (K) is the resistance to compression. Other terms used to describe the shear modulus and the bulk modulus are rigidity and incompressibility, respectively. Bulk modulus is the ratio of hydrostatic stress to volumetric strain. Shear modulus is the ratio of extensional stress to extensional strain. The bulk modulus and the shear modulus equations are given below:

$$K = \frac{\Delta P}{\Delta V / V} \tag{1}$$

$$\mu = \frac{\Delta F / A}{\Delta L / L} \tag{2}$$

where ΔP is the pressure change, V is the volume, ΔV is the volume change, ΔF is the shearing force, A is the cross-sectional area, L is the shear plane distance, and ΔL is the shear displacement.

The rock or fluid properties that are changing in this project are the bulk modulus and the density. These properties change because there is a change of fluid from oil to gas and solvent. The shear modulus remains the same. Also, the temperature and the pressure do not have a significant effect on the changing bulk modulus and the changing density. Also, the porosity remained the same for this project. The rock and fluid properties can be linked to the seismic properties, which are the P-wave velocity and the S-wave velocity.

We begin with the basic equations that show the relationship between the seismic velocities and the elastic parameters.

$$V_P = \sqrt{\frac{K + (4/3)\mu}{\rho}} \tag{3}$$

$$V_S = \sqrt{\frac{\mu}{\rho}} \tag{4}$$

where V_P is the P-wave velocity, V_S is the S-wave velocity, and ρ is the density. Bulk modulus is affected by a change of fluid within the pore space of a rock but the Gassmann equation assumes that the shear modulus is not affected (at low frequencies). Fluid substitution is when one pore fluid is substituted for another pore fluid. Fluid

substitution is important for time-lapse analysis because most time-lapse case studies are for reservoir depletion. Reservoirs are depleted by one fluid replacing another fluid. In this project, the injected gas and solvent replace the oil in the pore spaces. The oil is then produced. The injected gas and solvent would cause the bulk modulus and the density to decrease.

2.3 The fluid substitution equations

The Gassmann (1951) equation (Equation 5) is used to calculate the effects of fluid substitution on the bulk modulus, which is then related to the velocity. Fluid substitution is used in time-lapse analysis to help predict the change in modulus with respect to the fluid changes.

There are various assumptions underlying the Gassmann equation. First, the rock is assumed to be isotropic and the mineral making up the rock are assumed to be homogeneous. Also, the pore spaces must be interconnected. Another assumption is that the frequencies must be low. This is so that the pore pressure has time to equilibrate during the propagation of the seismic wave (Hirsche and Hirsche, 1998; Smith et al., 2003). The pore pressure equilibrates when the pore fluids have sufficient time to flow to other pores. The Gassmann equation is:

$$K_{sat} = K_{dry} + \frac{(1-\frac{K_{dry}}{K_s})^2}{\frac{\varphi}{K_{fl}} + \frac{1-\varphi}{K_s} - \frac{K_{dry}}{K_s^2}} \qquad (5)$$

where K_{sat} is the bulk modulus of a rock saturated with fluids, K_{dry} is the bulk modulus of a dry rock, K_{fl} is the bulk modulus of the fluids, K_s is the bulk modulus of the solid

mineral making up the rock, and φ is the porosity. The dry bulk modulus, K_{dry}, is not for a completely dry rock. The rock should have a small amount of moisture present (Mavko et al., 1998). After substitution with a new fluid, a new fluid modulus is obtained and thus a new bulk modulus (K_{sat}) is obtained. Therefore, a new velocity can be determined.

Two different formulae have been used to compute the bulk modulus of a fluid, giving different results for K_{fl}. They are:

$$K_{fl} = S_w K_w + S_o K_o + S_g K_g + S_{sol} K_{sol} \tag{6}$$

$$\frac{1}{K_{fl}} = \frac{S_w}{K_w} + \frac{S_o}{K_o} + \frac{S_g}{K_g} + \frac{S_{sol}}{K_{sol}} \tag{7}$$

where K_w, K_o, K_g, K_{sol} are the bulk modulus of water, oil, gas and solvent, respectively. S_w, S_o, S_g, S_{sol} are the saturation of water, oil, gas and solvent, respectively. These saturation values are expressed as a fraction of the total fluid content. The sum of the saturation values is 1. Equation 6 is the arithmetic average, also known as the Voigt average (patchy saturation), and Equation 7 is the harmonic or the Reuss average (homogeneous fluid distribution). The Voigt method gives the upper bound value while the Reuss method gives the lower bound value. Since we do not know how the fluids are distributed within the pore spaces, we will take an average of the upper value and the lower value to determine K_{fl}.

The density, ρ, also changes when one pore fluid is substituted with another. The density is determined by:

$$\rho = \rho_s(1-\varphi) + \rho_{fl}\varphi \tag{8}$$

where ρ_s is the density of the solid mineral making up the rock and ρ_{fl} is the density of the fluids. The density of the fluids is determined with the equation:

$$\rho_{fl} = S_w\rho_w + S_o\rho_o + S_g\rho_g + S_{sol}\rho_{sol} \tag{9}$$

where ρ_w, ρ_o, ρ_g, ρ_{sol} is the density of the water, oil, gas and solvent, respectively.

Other equations used for fluid substitution are the Batzle and Wang equations (1992). They are a set of equations used to determine the values for the individual fluid densities (ρ_w, ρ_o, ρ_g, ρ_{sol}) and for the individual fluid bulk modulus (K_w, K_o, K_g, K_{sol}) based on the reservoir conditions. The parameters needed for these calculations are: pressure, gas gravity, temperature, oil gravity and gas-oil-ratio. The Batzle and Wang equations are summarized in Appendix A.

2.4 Seismic parameters affected by other factors

2.4.1 Pressure

The seismic parameters, mainly the seismic velocity and the density, are affected by pressure, temperature, fluid type, and porosity. Wang's (2001) paper and Mavko et al.'s (1998) rock physics handbook provide a good summary of rock physics. Another parameter is

$$\sigma = S - p \tag{10}$$

where σ is the net or the effective pressure, S is the overburden pressure, and p is the pore pressure. Usually the overburden pressure remains the same in time-lapse seismic but the pore pressure will change during production. A decrease in pore pressure would mean an

increase in net pressure. Increasing net pressure in the reservoir would cause the velocity to increase and the density to increase.

Both fluid changes and pressure changes can be detected on time-lapse seismic data. Two methods are used to differentiate between seismic changes due to fluid saturation and seismic changes due to pore pressure. The first method assumes that pressure and saturation affects the AVO (amplitude variation with offset) slope and intercept in different ways (Landro et al., 2003, Landro, 2001). The other method assumes that pressure and saturation affects the P- and S-wave impedances in different ways (Meadows, 2001). V_S is insensitive to fluid saturation but is sensitive to pore pressure increase and thus would be a good discriminator between fluid changes and pressure changes (Wang et al., 1998). According to an engineer working on this reservoir, the pressure change in the Rainbow B pool, from 1987 to 2002, is not more than 80 kPa, which is not enough to be significant (L.Carr, personal communications, 2003). Therefore, pressure changes are not a factor in this project.

2.4.2 Temperature

A temperature increase would cause both the seismic velocity and the density to decrease. Temperature changes are very important in steam injection recovery projects but temperature changes are not significant in this project since only solvent and gas are injected into the reservoir.

2.4.3 Fluid type

The change of fluid type also affects the seismic parameters. Gas and solvent are both injected into the Rainbow B reservoir to displace the oil. Both gas and solvent have

a lower fluid bulk modulus than the oil. Also, the solvent in this study behaves more like gas than like oil. Gas and solvent would cause the compressional velocity and the density to decrease. But, the amount of gas saturation is not as important. A 5% gas saturation can increase the reflection amplitude significantly but additional amounts of gas may not change the reflection amplitude much (Domenico, 1974). Generally, a rock saturated with 100% gas and a rock saturated with 5% gas would have similar appearance on seismic data.

2.4.4 Porosity

An increase in porosity would cause a decrease in the velocity and the density. The porosity is not the major factor affecting the velocity (Wang, 2001). Rather, the pore geometry or the pore shape is the major factor affecting the seismic properties. Pore geometry that is crack-like or has a low aspect ratio cause a rock to be more sensitive to fluid changes. A rock with vuggy porosity is also more sensitive to fluid changes.

2.4.5 Other

The velocity for the carbonate rocks is not as dependent on the depth of the reservoir as siliciclastic sediments (Eberli et al, 2003). Also, unlike siliciclastic sediments, clay content has very little effect on the velocity especially if it is less than 5% of the rock weight (Eberli et al., 2003).

2.5 Conclusion

The Gassmann equation is one of the most commonly used equations to calculate fluid substitution. In this study, the fluid, oil, is being substituted with gas and solvent. Other equations presented in this chapter will be used for later calculations.

Temperature, pressure, fluid type, and pore geometry have a significant effect on fluid related changes in seismic. The temperature and pressure change in the Rainbow B pool are fairly negligible in this study and will not be discussed any further. The fluid types injected are gas and solvent, which cause the velocity and the density to decrease because the gas and solvent have a lower fluid modulus and lower density than oil. The porosity is not as important as the pore geometry in the Rainbow pool.

Chapter Three: RAINBOW B BACKGROUND

3.1 Introduction

In order to determine the location of the injected fluids, it is important to discuss the geology of the reservoir. The reservoir engineering aspect will also be discussed. Based on geological and engineering data entered into the reservoir simulation, a gas and solvent thickness map is made. This map is used to describe the amount of injected fluids believed to be in the reservoir. The geology and engineering data are found at the well locations but the data are interpolated between the wells locations. However, time-lapse seismic covers areas between the well locations. The geological and engineering data in this chapter will later be used to compare to the time-lapse seismic results. The last section to be discussed in this chapter is the background information on the seismic data.

3.2 Geological setting

The Rainbow B pool is an atoll reef or a rim dominated buildup located in northwest Alberta, township 108-109, range 8 W6M (Figure 3). The map view shows that there is a north lobe and a south lobe. An area referred to as the "saddle point" connects the lobes. The reef is 5.6 km long and 2.1 km wide at its widest point. The average thickness of the reef is 200 m and it is located at a depth of 1760 m (or -1275 m above sea level). The pool is producing oil from the Middle Devonian Keg River formation. The Keg River formation is overlain by the Muskeg member, which is made of impermeable evaporites, and is underlain by calcareous shales and argillaceous limestones (Figure 4) (Hirsche and Hirsche, 1998). The depositional environment in the

interior of the reef is lagoonal (Figure 5). A lagoonal environment is a quieter setting and therefore is lower in porosity than the outer edges of the reef. The average porosity within the B pool is 8% while the average permeability is 460 mD. The majority of the reef is dolomitized. Dolomitization is the process where limestone is converted to dolomite. This process increases the porosity of the rock. Figure 6 shows a photograph of core from well 7-10. More photographs of core depicting porosity types are found in Appendix B. The highest porosity is on the northeast side of the reef. A suggested reason for this is that prevailing winds came from the northeast (A.Laflamme, personal communications, 2003).

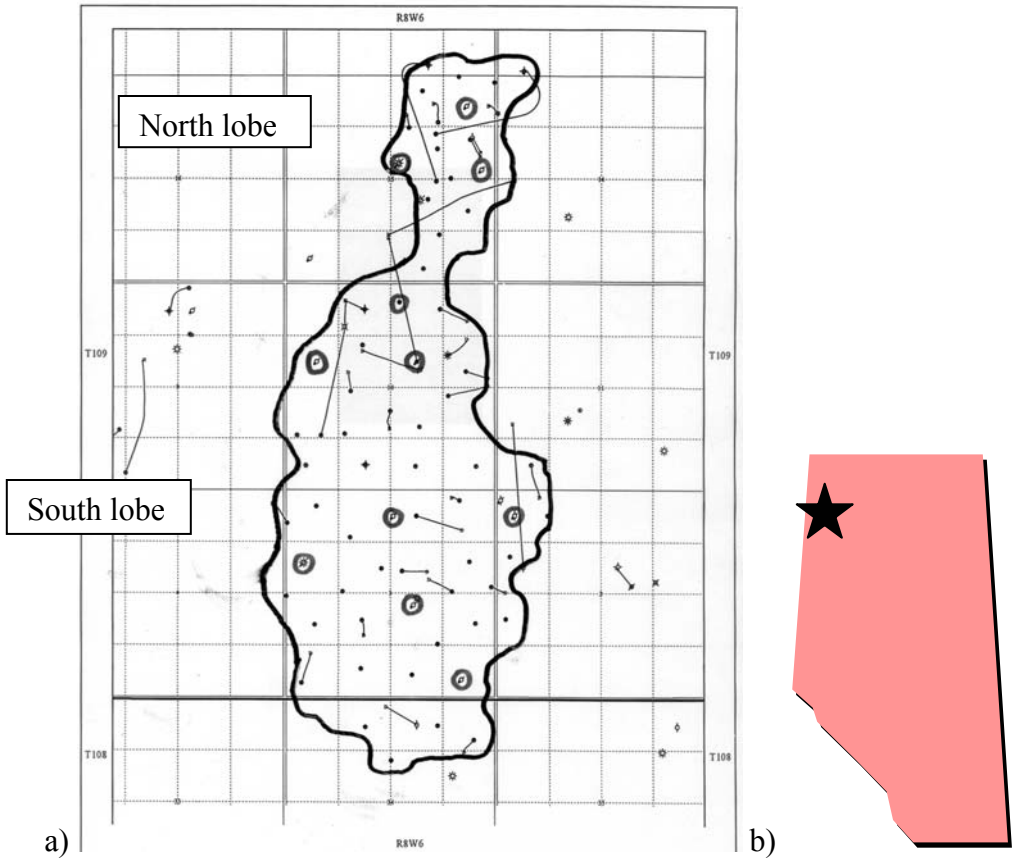

Figure 3. a) Map of the Rainbow B reef edges. Injection wells are circled. b) location in Alberta, Canada

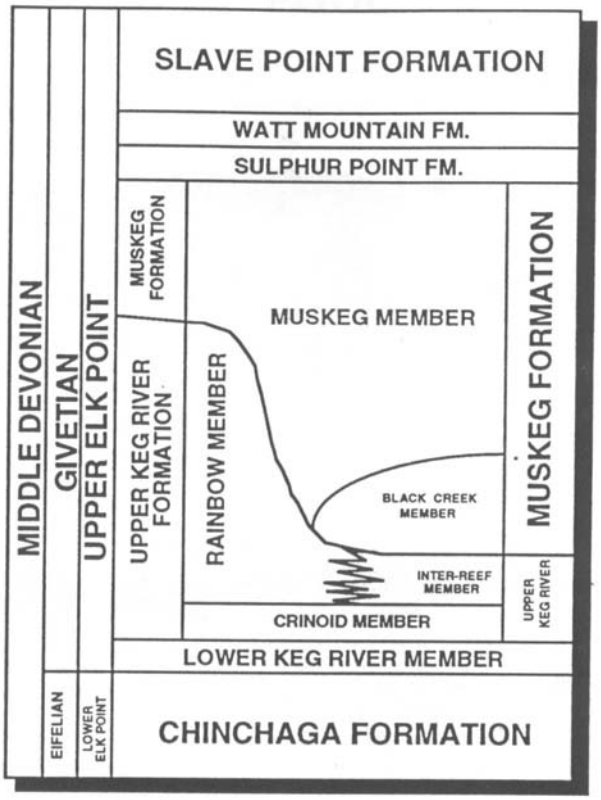

Figure 4. Stratigraphic chart. The Keg River formation is producing oil. The Muskeg member is the seal rock. (Laflamme, 1993)

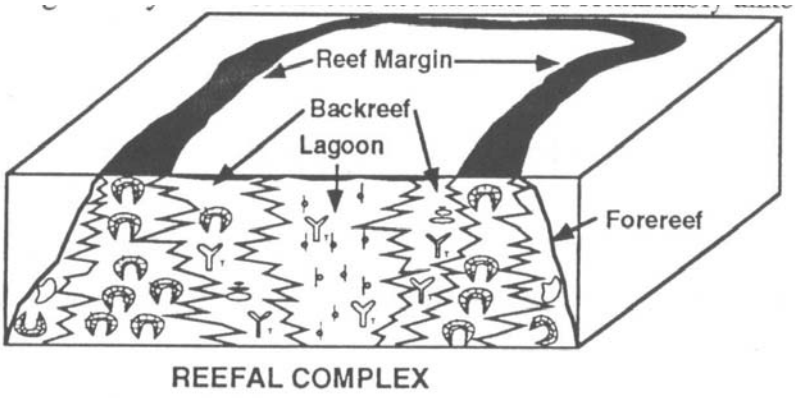

Figure 5. Model of the Rainbow B reef. The interior of the reef is a quieter lagoonal environment while the reef margin is a higher energy environment. The porosity is higher near the edges of the reef. (Laflamme, 1993)

Figure 6. Photograph of core from well 7-10. Porosity type seen here, from left to right, is zebroidal, vuggy, and intercrystalline. Average porosity is 8%.

The Rainbow B reef is very heterogeneous. The porosity varies within the reef both vertically and horizontally. The porosity can be visualized more easily in map view. Figure 7 shows a map view of the weighted average porosity over all the layers. For an example of how weighted averages are calculated, please refer to Appendix C. Each grid block in the reservoir simulation has a certain porosity value and the porosity values in all the layers were averaged for each location. Porosity data were taken from the geological information at the well locations and were interpolated between the wells. Note that the north lobe has higher porosity and also the edges of the reef have higher porosity than the interior.

Within this study, the pore geometry is more important than the magnitude of the porosity of the pool. The main porosity types can be broken down into two categories: vuggy porosity and intergranular porosity.

Intergranular porosity is defined as the porosity between the grains (Laflamme, 1993). The pore aspect ratio of this type of porosity is usually high because the pore

space is somewhat round. Also, the pore spaces are usually interconnected amongst the grains. Intergranular porosity includes intercrystalline porosity.

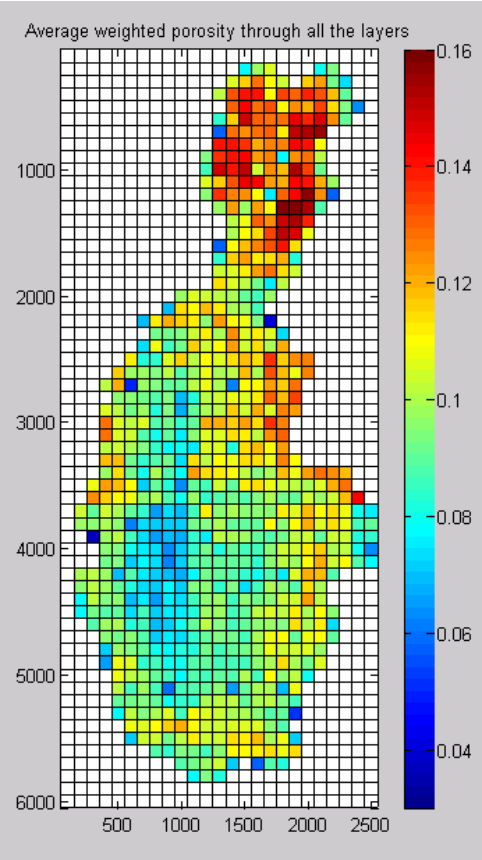

Figure 7. Porosity map: weighted average of all the layers. There is higher porosity in the north lobe and higher porosity near the edges of the reef. (Data from reservoir simulation) The average porosity is 10% with a standard deviation of 4.5%.

Vuggy porosity includes mesovug porosity and zebroidal porosity. Zebroidal porosity is a term describing porosity zones that have a striped appearance like a zebra. The zones are made of saddle dolomite interlayered with replacement dolomite (Laflamme, 1993). Zebroidal porosity zones are very porous and the fluids in those zones tend to flow laterally or spread horizontally. The majority of the reef has vuggy type porosity. Fluid effects are more significant in vuggy type porosity. Also, the vuggy

zones have a lot of cracks and fractures, which tend to weaken the rock. The cracks and fractures have a pore aspect ratio that is low, which makes the fluid effects more significant.

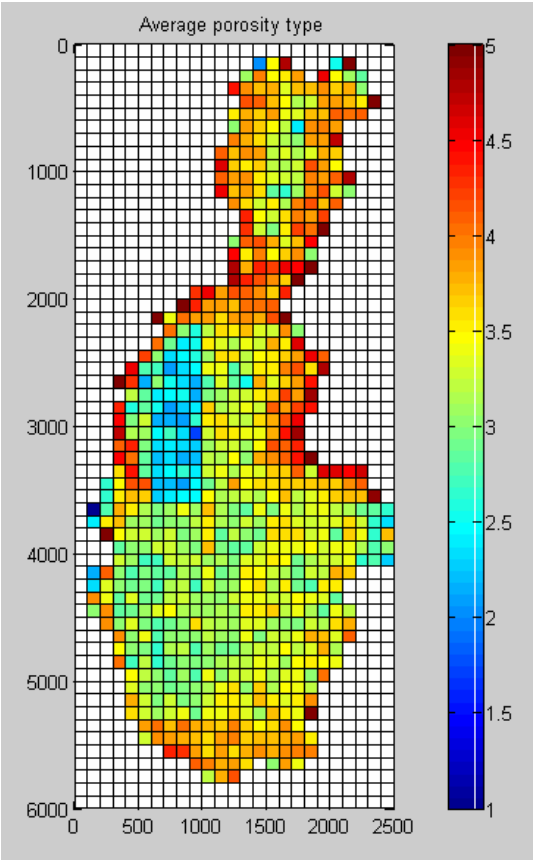

Figure 8. Porosity type map: average of all the layers (data from the reservoir simulation)

LEGEND
Porosity type 5: mostly large vugs
Porosity type 4: medium vugs
Porosity type 3: Predominantly vuggy with secondary intergranular matrix
Porosity type 2: Predominantly intergranular with reservoir quality porosity
Porosity type 1: Entirely intergranular with downgraded porosity

The porosity type has more of an effect than the magnitude of the porosity. Each of the 61, 500 grid blocks in the reservoir simulation was described by a porosity type value. Figure 8 shows the porosity type averaged over all the layers. Although averaging a porosity type is not entirely feasible, this method consolidated the porosity type from the 61 500 grid blocks and allowed the porosity type to be displayed in map view. Five porosity types were entered into the reservoir simulation. They are described in the legend in Figure 8. The outer edge of the reef is mostly vuggy. In the northwest corner of the south lobe is a zone that is mostly intergranular.

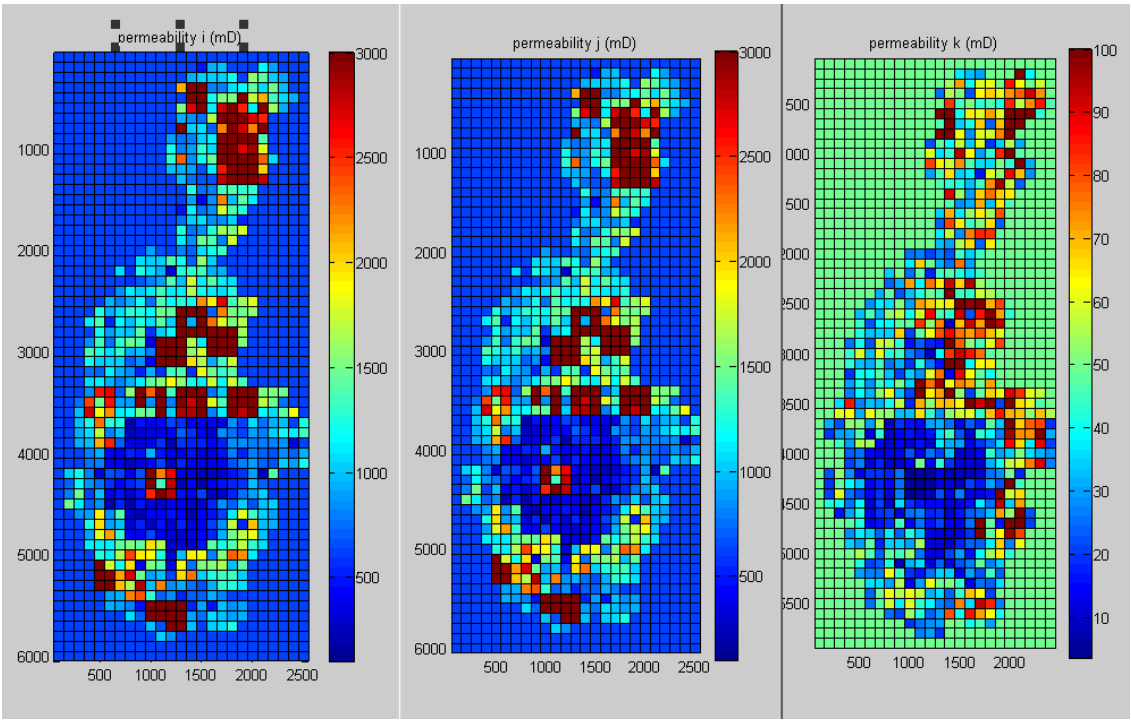

Figure 9. Permeability map: data averaged through all the layers. The first two maps on the left represent the horizontal permeability while the third map represents the vertical permeability. (Permeability data used in the reservoir simulation)

The permeability data put into the reservoir simulation results are also averaged and shown in map view (Figure 9). The horizontal permeability maps show zones of higher

permeability in dark red. The vertical permeability map shows the highest permeability on the east edge of the reservoir.

3.3 Reservoir description

Table 1. Rainbow B pool timeline

Date	Process	Description
1965, November	Primary production	Oil produced by natural drives
1968, March	Secondary production	Pool waterflooded
1984, June	Tertiary production begins	Solvent injected first into the north lobe, then through south lobe
1987, January	3D seismic data acquired	10 m solvent bank formed
1991, October	Tertiary production continued	Solvent injection stopped, miscible gas injected
2002, January	3D seismic data acquired	30 m solvent bank formed

Husky Energy is the operator of the pool, which has been producing oil since 1965. The OOIP (original oil in place) is 43.750 * 10^6 m^3. During primary production, 1.6% of the original oil in place (OOIP) was recovered while 36.5% OOIP was recovered during secondary production (Fong et al., 1991). The pressure in the reservoir during production never reached bubble point, which is at 10 845 KPa, so the dissolved gases in the oil did not come out of the solution. Also, there was never a gas cap in the pool. Table 1 shows the timeline for the Rainbow B pool. To further enhance oil recovery, miscible gas and solvent are injected into the top of the reservoir (Figure 10). The gas injected is mainly methane with some CO_2 in it. The solvent helps remove the residual oil from the reservoir and is analogous to dishwashing soap removing grease from a dinner plate. The solvent is injected first and then a lean gas is injected into the reservoir

to push the solvent bank down. Time-lapse analysis will help infer the injected fluid locations in the reservoir. There are currently 11 injection wells in the reservoir. Table 2 shows the injection wells and the times of injection. Table 3 shows some of the reservoir information. Pressure did not change by more than 80 kPa in the reservoir after injection. This may be because the high permeability of the reservoir equilibrates the pressure differences (L.Carr, personal communications, 2003).

Figure 11 shows a north-south cross-section of the fluid contacts from the simulation results in January of 1987. The original oil water contact (OOWC) was –1380.8 m. The approximate saturation values in each fluid zone are shown in Table 4.

Figure 12 is the same cross-section for the year 2002. More gas and solvent have been injected and most of the water has been produced. The thickness of the gas and the solvent saturated grid blocks in Figure 11 and 12 can also be represented in map view (Figure 13). I created Figure 13 by summing the grid blocks over the layers saturated with gas and solvent. Then the difference is taken of the total thickness between 1987 and 2002. According to Figure 13, there appears to be a lot of gas and solvent in the northeast part of the reservoir.

Table 2. Injection wells and the times of injection

Wells	Time of injection of gas and solvent
3/13-2-109-8W6M	December 2001 - present
1-3-109-8W6M	June 1984 - present
7-3-109-8W6M	April 1992 - present
12-3-109-8W6M	June 1984 – present
15-3-109-8W6M	January 1989 – present
2/10-10-109-8W6M	April 2002 – present
12-10-109-8W6M	June 1985 – present
15-10-109-8W6M	June 1984 – September 1993
9-15-109-8W6M	April 1983 – present
10-15-109-8W6M	January 1985 – present
16-15-109-8W6M	August 1987 – present

Table 3. Reservoir information (Nagel et al., 1990)

Pressure	17.2 MPa
Temperature	87 °C
Original oil in place	$43 * 10^6$ m^3
Maximum reservoir thickness	233 m
Average porosity	8 %
Average permeability	460 mD

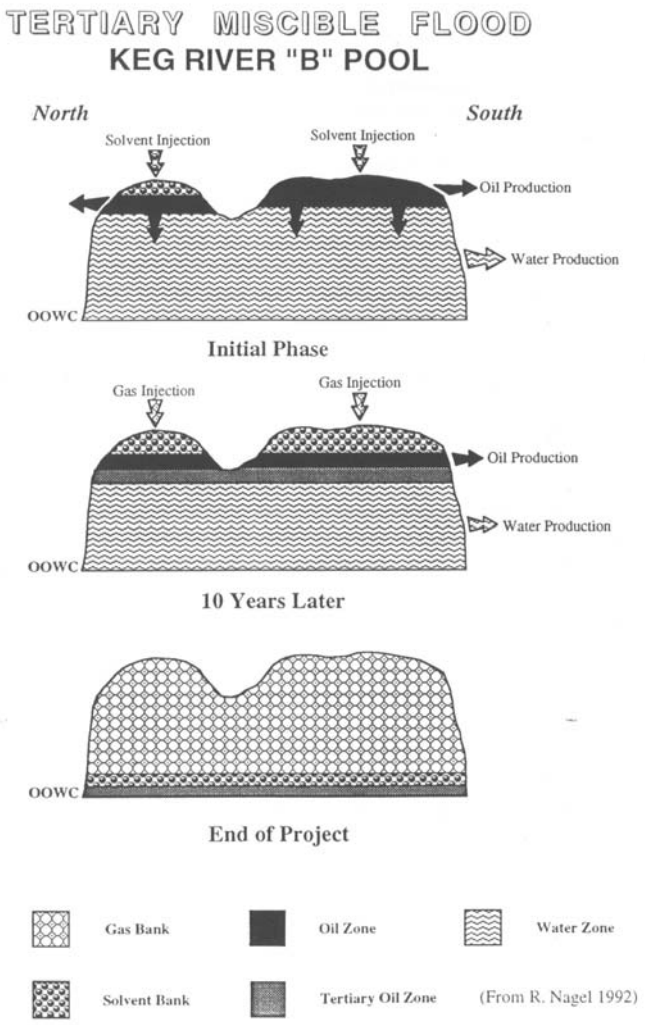

Figure 10. Tertiary miscible production process: The solvent is injected first into the top of the reservoir, and then the gas is injected to push the solvent bank downwards. During this process, oil and water are produced. (Nagel et al., 1990)

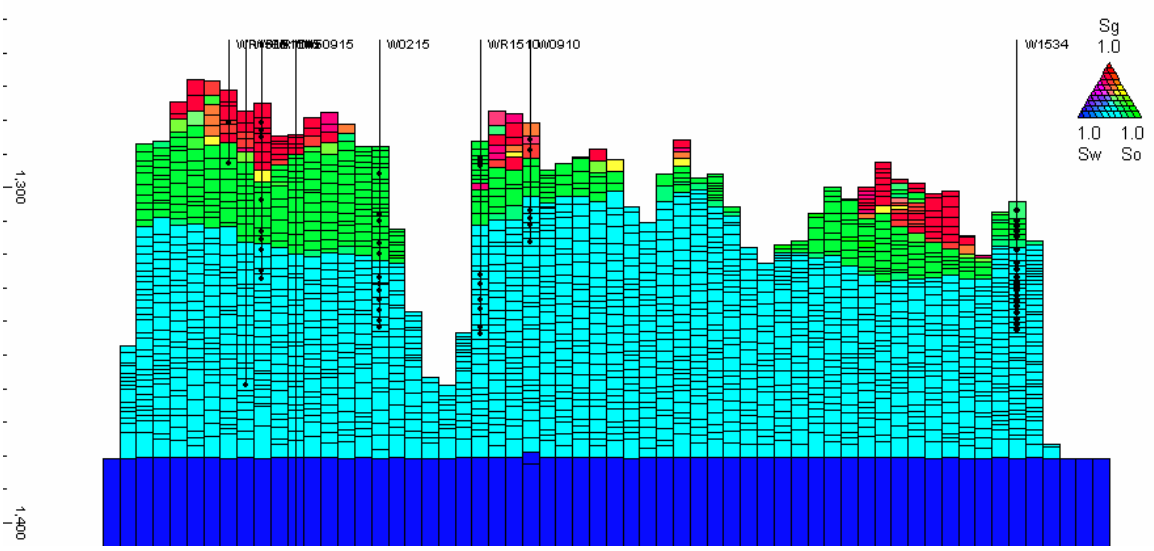

Figure 11. North-south cross section of the fluid contacts in 1987-01-01. Light blue represents the grid blocks saturated mainly with water. Green represents the oil saturated grid blocks. Red represents the gas & solvent saturated grid blocks.

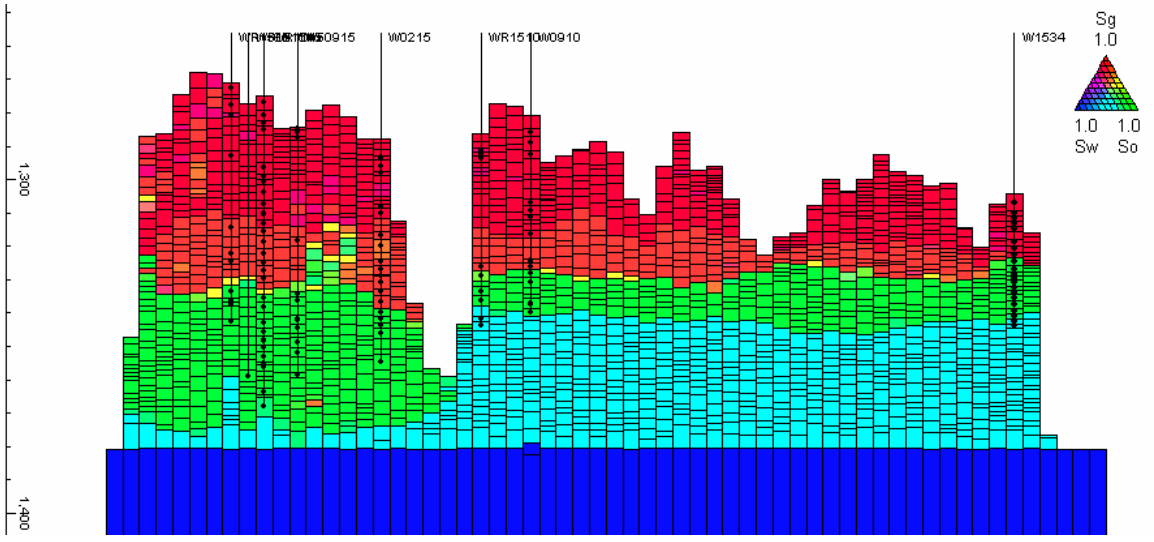

Figure 12. North-south cross section of the fluid contacts in 2002-01-01. Light blue represents the grid blocks saturated mainly with water. Green represents the oil saturated grid blocks. Red represents the gas & solvent saturated grid blocks.

Table 4. Approximate saturation values in each zone

Zones	Water saturation (S_w)	Oil saturation (S_o)	Gas saturation (S_{gas})	Solvent Saturation (S_{solv})
Water zone	0.54	0.46	0	0
Oil zone	0.10	0.90	0	0
Gas zone	0.12	0.15	0.73	0
Solvent zone	0.10	0.20	0	0.70

a) b) c)

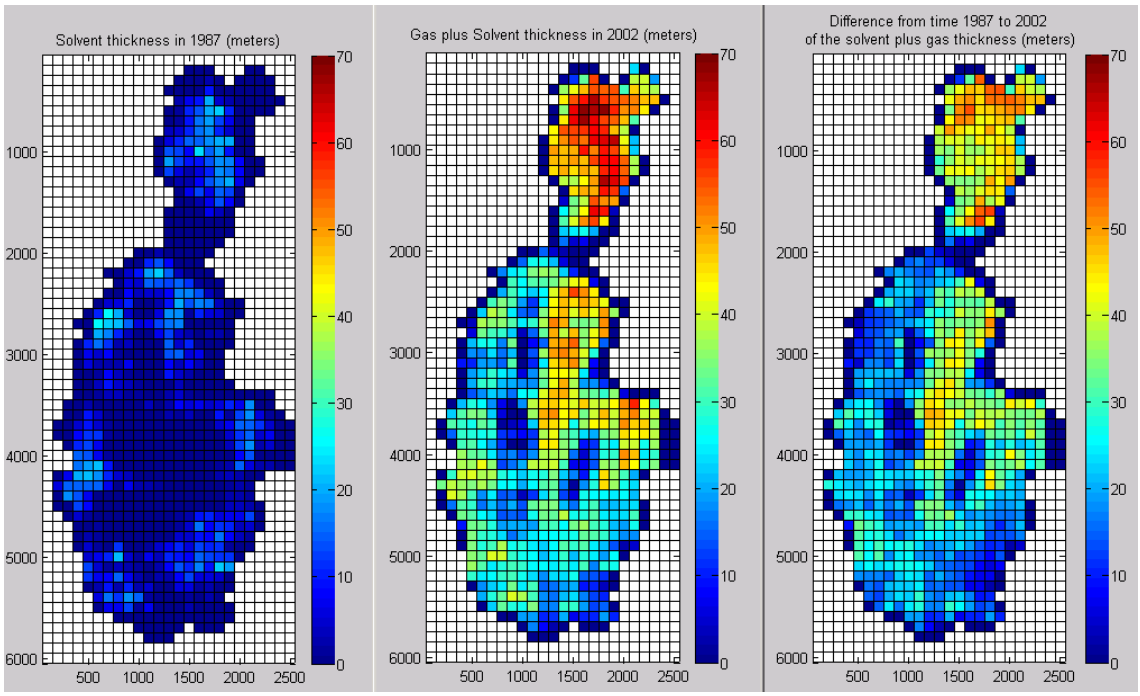

Figure 13. a) Gas plus solvent thickness summed over all the layers in 1987. b) Gas plus solvent thickness summed over all the layers in 2002. c) Difference of gas plus solvent thickness summed over all the layers from 1987 to 2002; results from the reservoir simulation

3.4 Seismic surveys

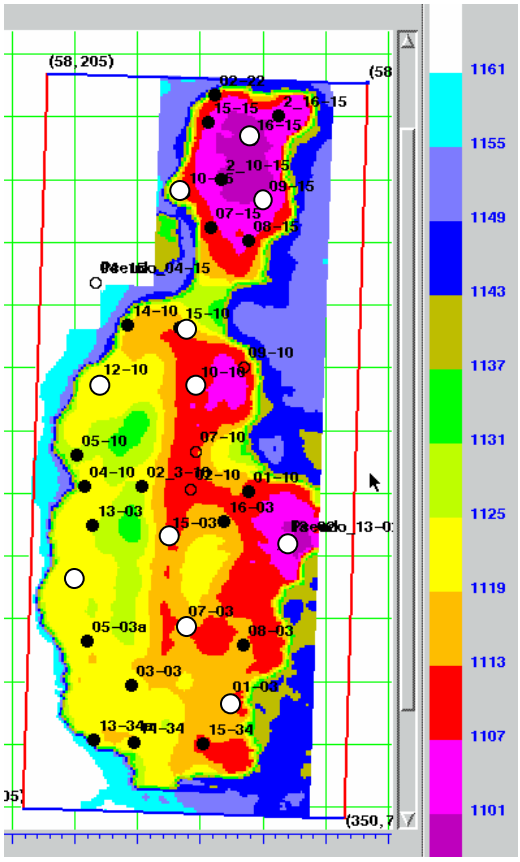

Figure 14. Time structure of the top of the Keg River (milliseconds)

Two 3D seismic surveys were acquired. The acquisition parameters are found in Appendix D. Some of the processing parameters are given in Table 5. The first survey was acquired in 1987. Gas injection had begun three years before the survey. An estimated solvent bank of 10 m had formed. Another 3D seismic survey was acquired after fifteen years of further gas injection. In June of 2002, the 1987 survey was reprocessed so that the processing parameters are the same as the 2002 survey. Also, the 1987 survey has been regridded to the 2002 survey. The in-lines are east-west seismic lines numbered 58 to 350 while the cross-lines are north-south seismic lines numbered 78

to 205. Figure 14 shows the time structure map of the top of the Keg River formation (the horizon picks are from the 2002 survey). Figure 15 is the isochron map from the

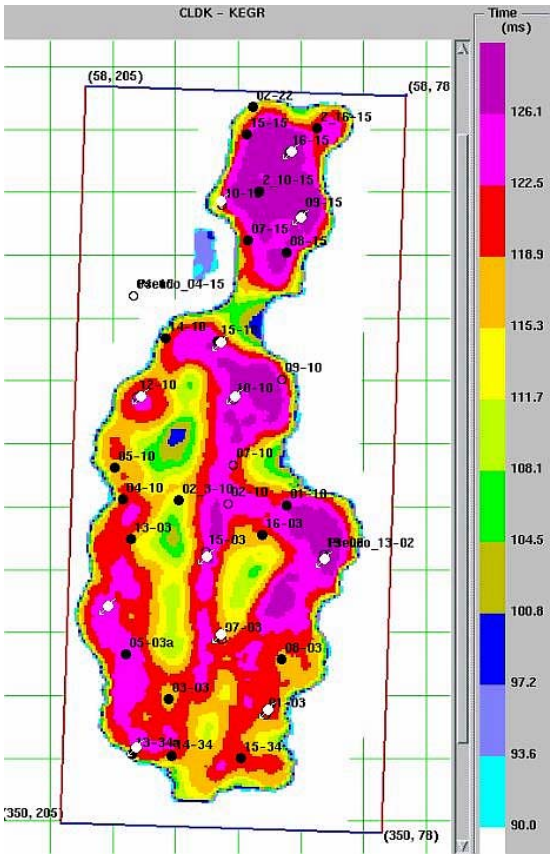

Figure 15. Isochron of the Keg River horizon to the Cold Lake horizon (milliseconds)

Keg River formation to the Cold Lake formation. The Cold Lake formation is a salt that is deposited during early Devonian times, before the deposition of the reef. On seismic data, the Cold Lake horizon is a flat trough event below the reservoir. The horizon picks are shown in Figure 16 and 17. The Slave Point and the Sulphur Point formation are picked as peaks and the Keg River and the Cold Lake formation are picked as troughs. Figure 16 shows a north-south cross section (cross-line 130) of the south lobe of the pool from data acquired in 1987. The 2002 survey along the same cross-section is shown in

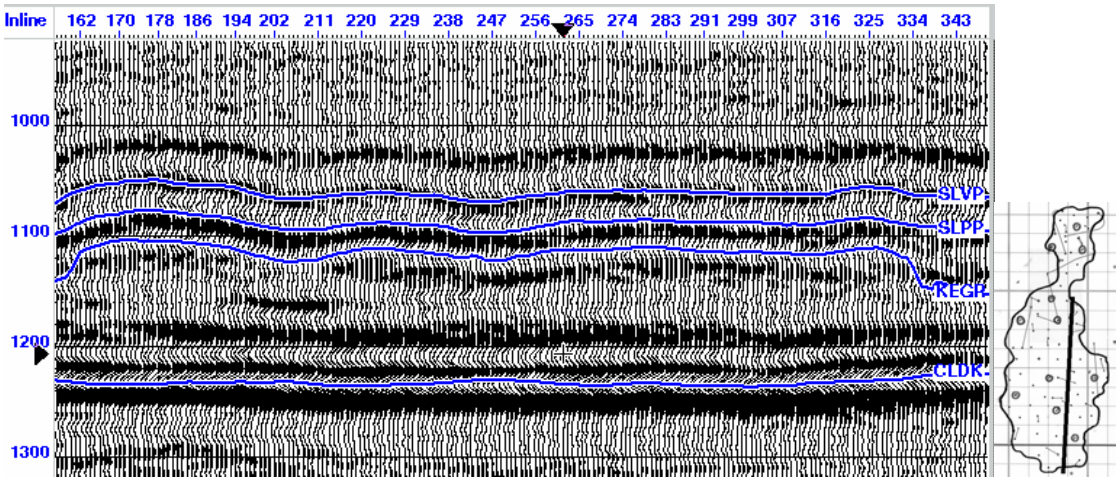

Figure 16. 1987 seismic data (Base survey). Cross-line 130 of southern lobe; SLVP is Slave Point, SLPP is Sulphur Point, KEGR is Keg River, CLDK is Cold Lake.

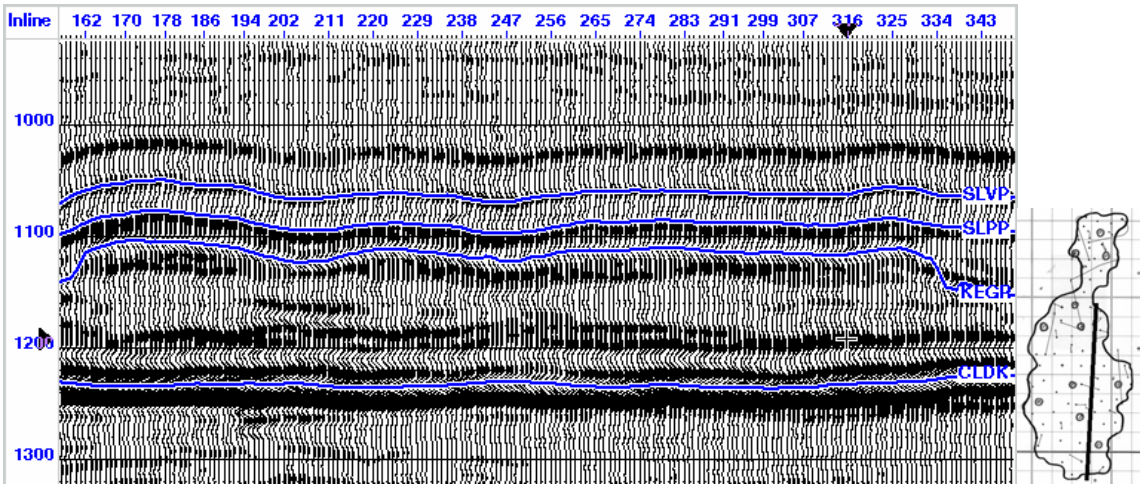

Figure 17. 2002 seismic data (Monitor survey). Cross-line 130 of southern lobe; SLVP is Slave Point, SLPP is Sulphur Point, KEGR is Keg River, CLDK is Cold Lake.

Figure 17. Note that the 2002 seismic data prior to time-lapse processing has higher frequency content than the 1987 survey. To infer this, the amplitude event at 1190 ms separates to two separate events from 1987 to 2002 (refer to Figure 16 and 17). Also, only the seismic traces within the Rainbow B pool are presented because the seismic

traces around the pool have been removed due to confidentiality. The offsets are also different for the two surveys. The fold is higher for the 2002 survey. Other differences are in the recording equipment, the acquisition geometry, and random noise differences. Consequently, it is necessary to do time-lapse processing, which will be explained in the next chapter.

Table 5. Processing parameters for the 3D seismic surveys

1987 survey	2002 survey
Acquired Dec 31, 1986 to January 25, 1987 Re-processed October 2002 20 m bin size Datum: 550 m; Replacement velocity: 2500 m/s Pre-stack Kirchoff migration Filter: 8-12-90-110 Hz but original filter prior to reprocessing was 4-8-70-80 Hz Surface consistent deconvolution Window 100-300 ms, 350-1300 ms Sample rate: 2 ms	Acquired February 12-20, 2002 Processed June 2002 20 m bin size Datum: 550 m; Replacement velocity: 2500 m/s Pre-stack Kirchoff migration Filter: 8-12-90-110 Hz Surface consistent deconvolution Window 100-300 ms, 350-1300 ms Sample rate: 2 ms

3.5 Conclusion

The Rainbow B pool is a reef that has higher porosity on the edge or rim of the reef than within the interior. However, the pore geometry has more of an effect on seismic fluid changes than the magnitude of the porosity. The porosity map, the porosity type map and the permeability map were presented. The results from the reservoir simulation showed the locations of the fluids: water, oil, gas and solvent. The thickness of the injected fluids from the reservoir simulation can be viewed in map view and will later be compared to the time-lapse analysis results. I made the maps in this chapter by taking data from the reservoir simulation. The seismic data and various seismic maps were also presented in this chapter. I made the time structure map and the isochron map by

interpreting horizons in the seismic data. The seismic data had already been processed but had not been time-lapse processed. The next chapter discusses the time-lapse processing that I performed.

Chapter Four: TIME-LAPSE PROCESSING PROCEDURE

4.1 Introduction

Stacked seismic 3D data from the Rainbow area were obtained for this time-lapse study. Unfortunately, they are not similar enough to be compared to one another. Although the seismic processing parameters are the same, there are differences in the acquisition parameters. Before the two seismic data sets could be compared, they have to be time-lapse processed to match one another in terms of acquisition geometry, phase, time, frequency and amplitude. In general, a wavelet operator is estimated to shape and match the reflection data of one survey to another (Ross et al., 1996). The crossequalized trace, which is the new trace, is calculated by convolving the input trace with a wavelet operator based on phase, time, frequency, and amplitude. Then, the two seismic data sets can be subtracted from one another to find the differences that should be due to the production effects only. The production effects in this study are due to the presence of injected gas and solvent. Please refer to Rickett and Lumley (2001) for more information on time-lapse processing, also sometimes known as crossequalization.

The newer survey (2002) is the Monitor survey and the older survey (1987) is the Base survey. The Base seismic data are lower in frequency than the Monitor seismic data so it is better to time-lapse process the Monitor data so that it matches the Base data. I do not recommend time-lapse processing the Base data to match the Monitor data because this may introduce high frequency noise into the Base data. However, in Appendix E, I have also time-lapse processed the Base data to match the Monitor data. The results are fairly similar because matching tends to occur in the common part of the frequency

spectrum from both surveys (K.Hirsche, personal communications, 2004). The time-lapse processing procedure consists of:

1. Regridding
2. Phase & Time Shift
3. Shaping Filter/Matched Filter
4. Crosscorrelation shallow statics/"Warping": used to interpret time differences
5. Time-Variant Shifts: used to interpret amplitude differences

The names and general procedure of these steps were taken from the help manual on the time-lapse processing software.

4.2 Regridding: step 1

Regridding matches the processing output geometry of one seismic survey to the other. Kelman Processing reprocessed the two 3D data sets so that the in-lines and cross-lines are numbered the same. Thus, this step is not necessary in this study. The data sets also have the same replacement velocity and the same datum.

4.3 Phase and Time shift: step 2

The next step is Phase & Time shift. This step estimates and applies a first order constant phase correction and a constant bulk time shift. Unfortunately, the time will be altered when the phase shifts are applied. To overcome this problem, both the time shift and the phase shift are estimated together via the Russell-Liang technique (Hirsche, 2002). To determine the time shift in this technique, a time-pick is made on the envelope amplitude of the crosscorrelation of the Base to the Monitor survey. To determine the phase shift, a pick is made on the instantaneous phase of crosscorrelation that corresponds to the time of the envelope maximum (Hirsche, 2002).

The design window chosen was 750-1100 ms, which is above the reservoir area. This area excludes the production zone and so the Monitor survey and the Base survey should be the same after this step, in terms of phase and time, in that design window. A phase shift and a time shift is estimated from this design window and applied to the Monitor survey. The correlation threshold chosen was 50%. This means that traces where the correlation is less than 50% are excluded. This is done to eliminate the matching of noise. A global average matching process is used so that there is only one phase and one time shift applied to all the traces. The global average matching process is better than the trace-by-trace process because the global option insures that any trace-by-trace variations are preserved (F.Ma, personal communications, 2002). A first order phase shift of –19.3 degrees and a time shift of –2.46 ms were calculated and applied.

As an aside, the design window can also be chosen to include the reservoir and the correlation threshold is chosen to exclude traces that are within the production zone so that those traces are not used to estimate the phase and time-shift. But because the seismic traces around the pool are removed due to confidentiality, it is better to use a design window above the reservoir.

4.4 Shaping filter/matched filter: step 3

The shaping filter step (also referred to as match filtering) derives and applies a shaping filter to the Monitor survey. This process is used to match the static time shift, the phase, the amplitude and the frequency content between the surveys by calculating a convolutional shaping filter based on a certain design window (Rickett and Lumley, 2001). This shaping filter step uses the Wiener-Levinson filtering algorithm. The Wiener shaping filter operator is derived using the crosscorrelation lags of the Base

survey to the Monitor survey, and using the autocorrelation lags of the Monitor survey (Yilmaz, 1987). Then the shaping filter is convolved with the Monitor survey. Again, a design window from 750-1100 ms is used and the processing used is the global average method.

A test was done to check whether or not the shaping filter step is necessary. This is discussed more thoroughly in Appendix E. Although the shaping filter appears harsh because it diminished the amplitude change and also diminished the frequency content, this step also helped match the amplitude data and the frequency content of one survey to the other. Thus, this step was included in the processing. When we compare the seismic data processed with a shaping filter and the seismic data processed without a shaping filter, we realize that the results are similar because the amplitude changes are in the same locations. Only the magnitude of the changes is different.

Another test was to see if the length of the shaping filter applied made a difference to the 2002 data set. 21 samples were used for the shaping filter instead of 81 samples. The length of the shaping filter does not appear to make a difference to the results.

4.5 Crosscorrelation shallow statics: step 4

The Crosscorrelation shallow statics step applies a time shift that is derived from cross correlation analysis. This procedure has also been referred to as applying a "warp", used to align mispositioned events (Rickett and Lumley, 2001). This procedure is different than step 1 (Phase & Time shift) because step 1 is not able to spatially position reflectors because of differences in NMO and migration velocity functions between the two surveys (Ross and Altan, 1997). Also, this warping procedure calculates the time shift by the trace-by-trace method rather than by the global average method.

Again, the window was designed above the zone of interest at 750-1100 ms. Thus, after this calibration step, the seismic data above the zone of interest should be exactly the same in both data sets since we assume that there are no production effects there. Since the data sets have been matched above the reservoir, then time-delay effects can be seen below the reservoir due to the presence of injected gas and solvent. This is because the replacement of oil with gas and solvent causes a velocity decrease in the reservoir. A time-delay test was also done to confirm that the seismic data were indeed the same above the zone of interest. The test indicated that the time-delays were less than 0.3 ms above the reservoir, which is acceptable. The time-delay results obtained after this step will be discussed in the next chapter.

4.6 Time variant shifts: step 5

The last calibration step is to apply Time Variant Shifts, which is similar to the procedure in the previous step except that more design windows are chosen so that the data is matched above, within, and below the reservoir. Since any time deficiencies are minimized, the data sets are subtracted from one another to obtain the amplitude differences. Sliding windows from 1000 – 1300 ms were chosen for the design window to accommodate all time deficiencies. Each window was 50 ms and incremented in steps of 25 ms. An amplitude change test was also done to confirm that the seismic data were indeed the same above the zone of interest. The test indicated that the amplitude changes were up to 50% above the reservoir, which is not acceptable. Since there is no production occurring above the reservoir, the changes should be close to zero. Nevertheless, the amplitude results will be discussed in the next chapter.

4.7 Conclusion

Prior to comparing the 1987 data set to the 2002 data set for fluid related seismic changes, time-lapse processing had to be applied. The time-lapse processing steps included regridding the data set, applying a phase and a time shift, applying a shaping filter, applying crosscorrelation shallow statics, and applying the time-variant shifts. These steps are necessary to match the 2002 data to the 1987 data in terms of acquisition geometry, phase, time or static correction, frequency and amplitude. Then the remaining differences between the two surveys should only be due to fluid related changes. In this study, regridding was not necessary because it was already done. The time-delay results were determined after applying crosscorrelation shallow statics and the amplitude change results were determined after applying the time-variant steps. These results will be discussed in the next chapter.

Chapter Five: RAINBOW B TIME-LAPSE ANALYSIS RESULTS

5.1 Introduction

Three different seismic changes were investigated: time-delays, amplitude changes, and impedance changes. To infer the location of gas and solvent, we need to understand the effect gas and solvent have on seismic data. Figure 18 is a schematic showing the reservoir prior to and after fluid injection. The replacement of oil with gas and solvent would cause a velocity and density decrease. Hence, a time-delay or time-sag can be detected below the production zone. Also, the presence of gas and solvent would cause an amplitude increase at the top of the Keg River horizon due to an increase in impedance contrast. In addition, an impedance decrease should occur within the zone of gas and solvent. Impedance is the velocity multiplied by the density. The results of the time-delay, the amplitude change and the impedance change are displayed in map form in this chapter.

5.2 Time-delay results

The time-delay results are determined after crosscorrelation shallow statics have been applied. Figure 19 shows the 2002 data before and after time-lapse processing. Note that the frequency content in the 2002 data after processing is lower. This is because the 2002 data set was made to match the lower frequency 1987 data set. Figure 20 represents the difference between the 1987 data set and the time-lapse processed 2002 data set. Note that the largest differences occur below the reservoir near the Cold Lake horizon at 1230 ms. These are the areas where there are time-delays. Time-delays can be easily detected at the Cold Lake horizon because it is a strong amplitude event below the

reservoir. It is easier to observe the locations of time-delay in the entire reservoir in the form of a map. To do this, the 1987 survey is crosscorrelated to the time-lapse processed 2002 survey using a window of 1200-1250 ms to determine the time-delay required to match the Cold Lake horizons in the Monitor to the Base survey. The time-delay results are shown in Figure 21. The purple colours on the map could be interpreted as locations where there has been a large accumulation of gas and solvent. The time-delays are found to cover most of the reservoir. Although the time-delays appear to be small and also less than the sample rate of 2 ms, they are still anomalous and correlate well to the injection wells.

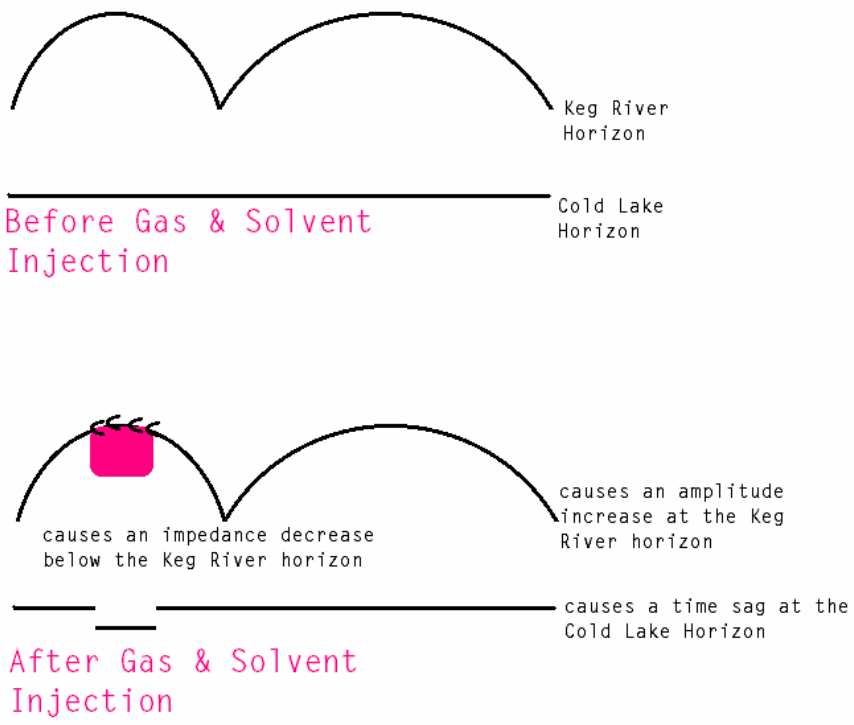

Figure 18. Schematic diagram of seismic results expected after the injection of gas and solvent.

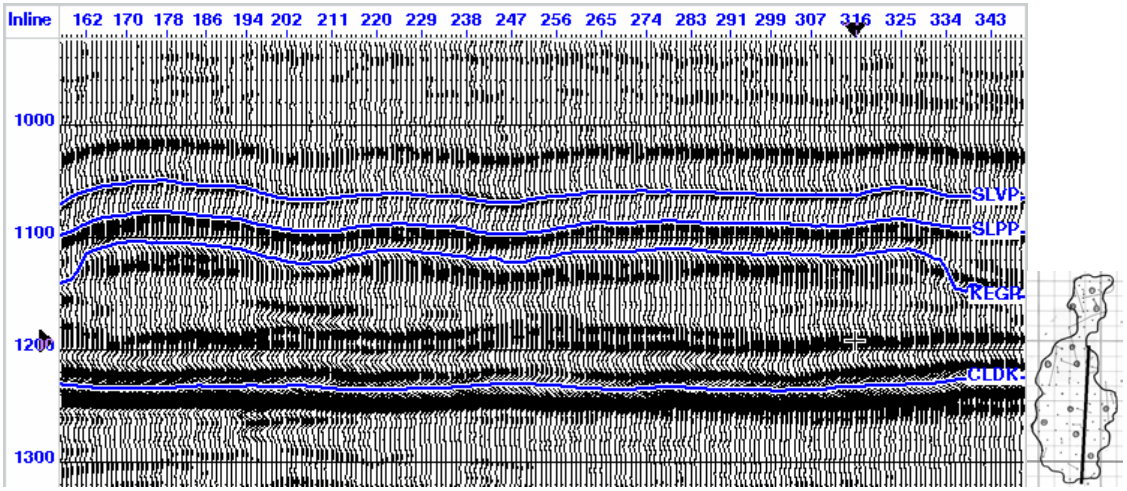

a)

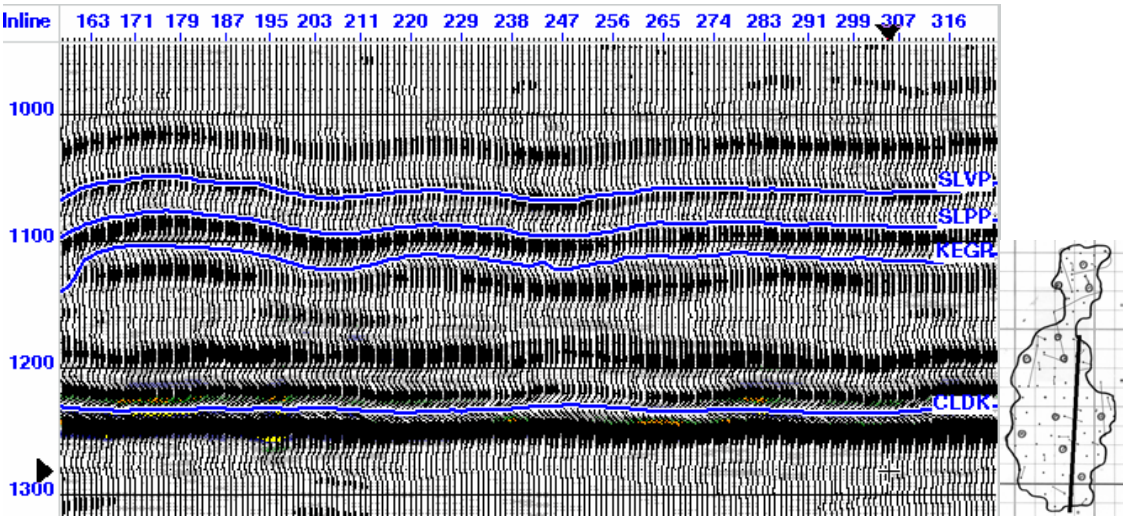

b)

Figure 19. a) 2002 seismic data before time-lapse processing at cross-line 130. b) 2002 seismic data after time-lapse processing at cross-line 130; Comparison of a) and b) reveal frequency differences. The data in b) now has lower frequency content than in a) because it was time-lapse processed to match the 1987 data set.

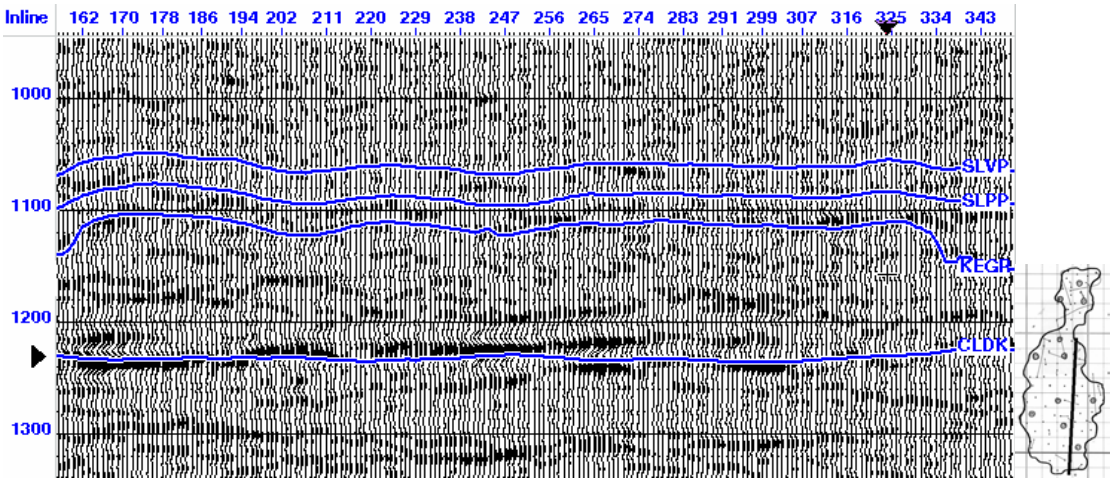

Figure 20. Difference between the 1987 survey and the time-lapse processed 2002 survey. High amplitude events at the Cold Lake horizon (CLDK) are due to time-delays beneath the production zones.

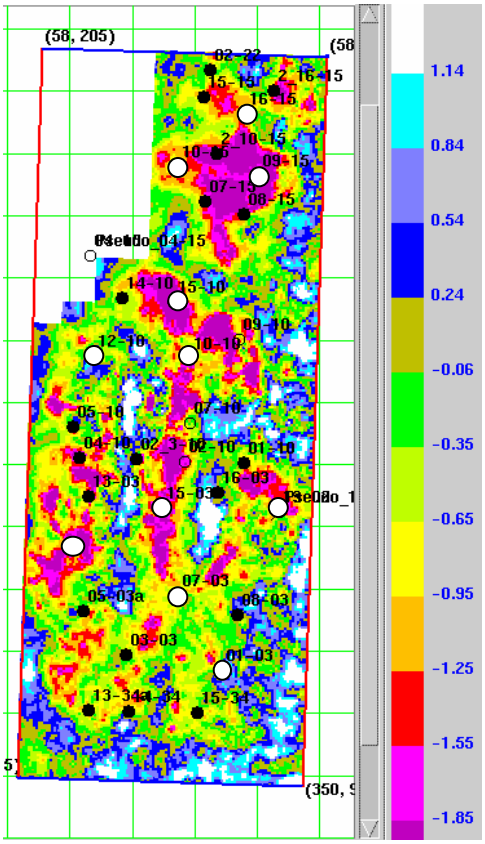

Figure 21. Time delay map calculated by taking the crosscorrelation for a window at 1200-1250 ms, which is centered on the Cold Lake horizon (milliseconds). Purple/pink areas could be interpreted as the time-delays in the reservoir.

5.3 Amplitude change results

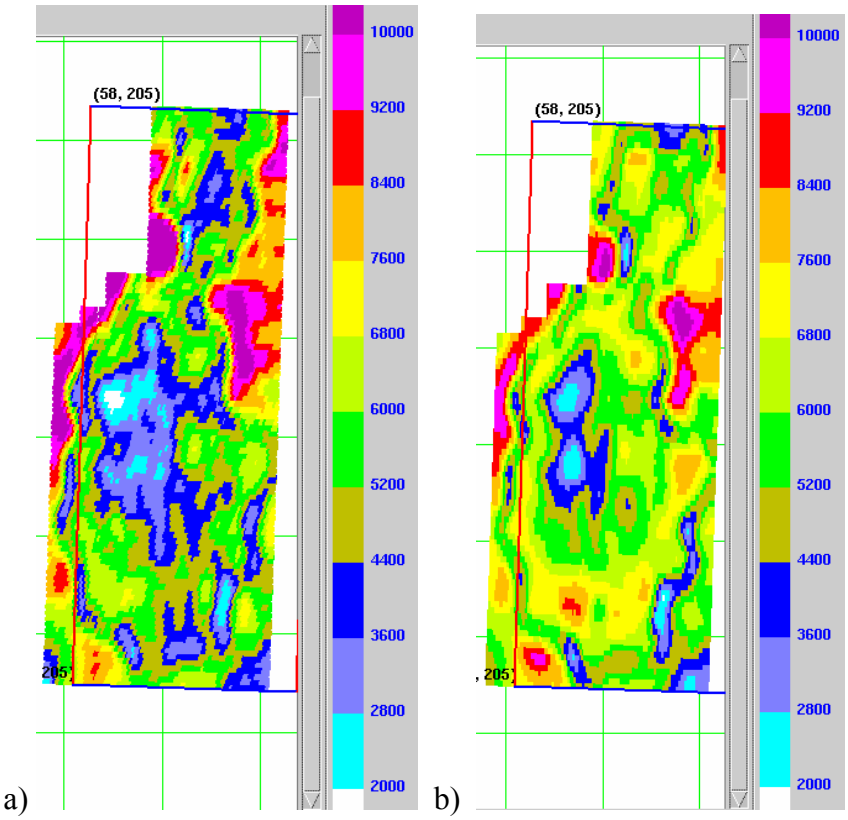

Figure 22. a) 1987 rms amplitude map at a window of 10 ms centered on the Keg River b) time-lapse processed 2002 rms amplitude map

After time-variant shifts are applied, amplitude differences at the top of the reservoir can be detected. The injection of gas and solvent replacing oil should cause an amplitude increase at the Keg River horizon due to an increase in impedance contrast. Figure 22 shows the increase in rms amplitude from 1987 to 2002. A difference map is made between the 1987 and the 2002 survey. Figure 23 shows a map of the normalized RMS amplitude differences with a window of 10 ms centered at the Keg River horizon. The purple/pink areas could be interpreted as areas where there has been an injection of gas and solvent. Unfortunately, this map does not correlate well to the time-delay map nor does it correlate well to the injection wells. The amplitude results may not be as

robust as the time-delay results because of the presence of noise, a lack of resolution due to the low frequency content, and perhaps processing errors. The low frequency of the seismic data in the zone of interest may prevent the amplitude results from being detected. Wavelength is the velocity divided by the frequency. If the frequency is 35 Hz, the velocity is 5500 m/s, then the wavelength in our zone of interest is 157 m. A wavelength of this size will not adequately resolve the amplitude changes.

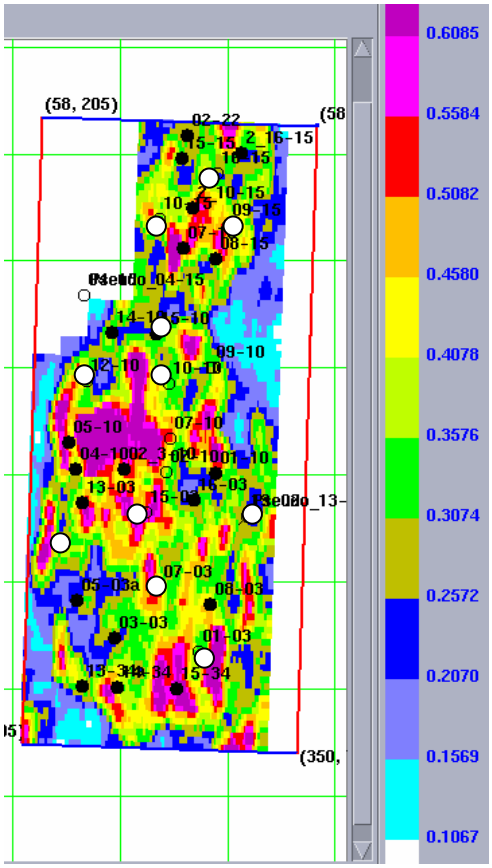

Figure 23. Normalized RMS averaged amplitude map of the difference between 1987 and 2002 with a window centered at 10 ms on the Keg River horizon. (fractional units)

The amplitude change results are also difficult to interpret because the reservoir already contained solvent prior to the first survey. This means that additional gas or

solvent injected may not have a significant effect on the amplitude. This is because the reflection amplitude may be the same whether there is 5% gas or 95% gas (Domenico, 1974). Tracking changes in amplitude does not seem to be a useful way of tracking solvent and gas distribution.

5.4 Impedance change results

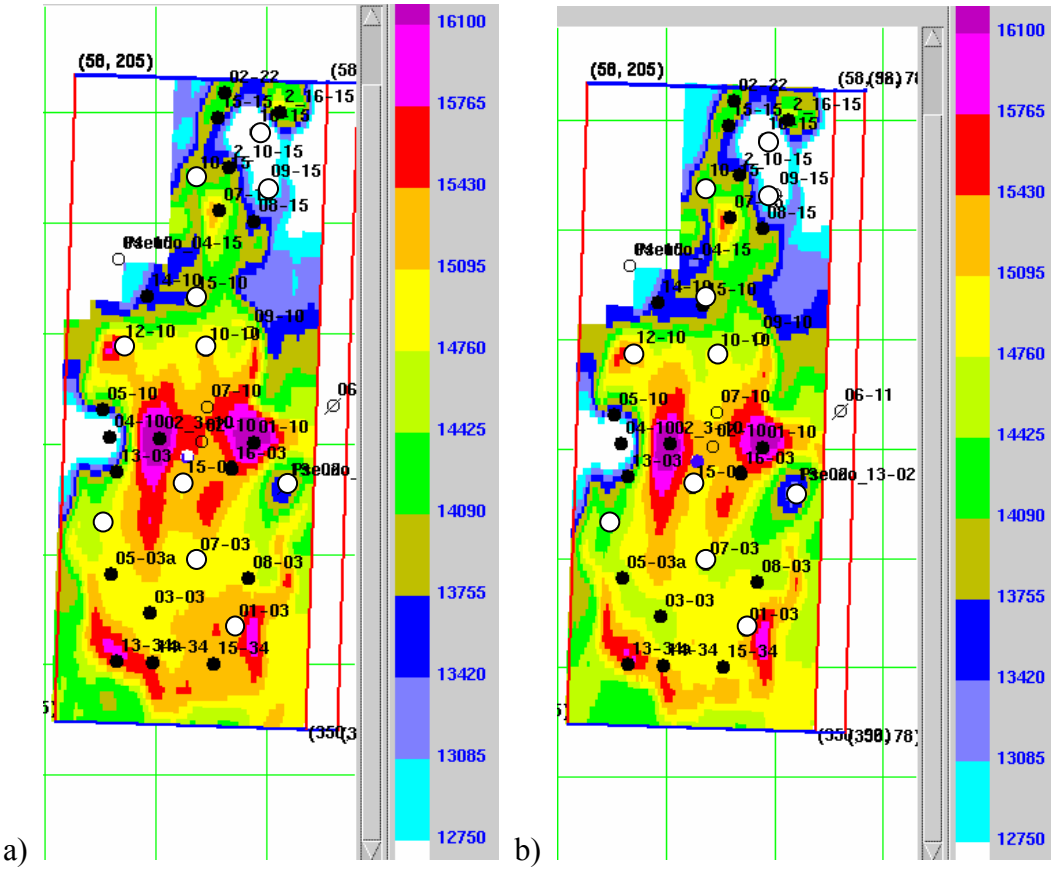

Figure 24. a) 1987 impedance data b) 2002 impedance data (arithmetic mean, window 20 ms below Keg River)

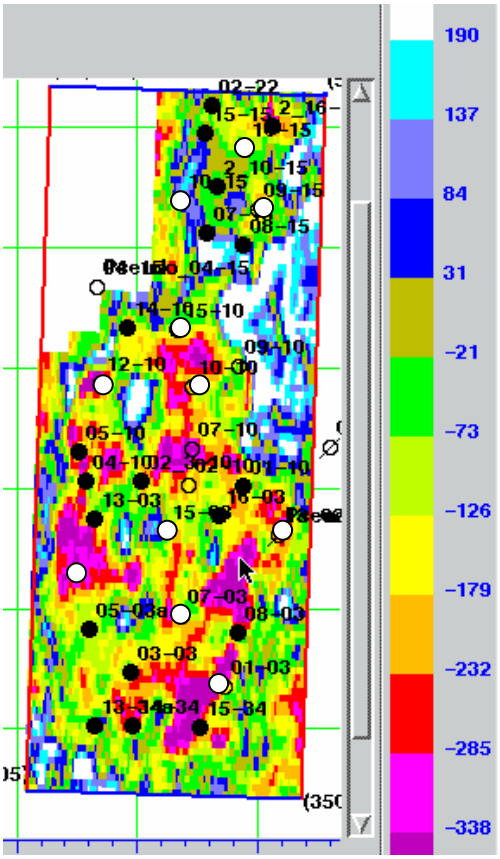

Figure 25. Difference of impedance between 1987 and 2002 (arithmetic mean, window 20 ms below Keg River)

To visualize the seismic stacked data in terms of the acoustic impedance, model-based inversion was applied. Impedance is the product of the density and the velocity. The injection of gas and solvent would cause the velocity and the density to decrease resulting in an impedance decrease. Slight impedance changes can be seen in the impedance maps from 1987 to 2002 (Figure 24). Figure 25 is a map showing the arithmetic mean of the impedance change from a window of 20 ms below the Keg River horizon. A window of 20 ms corresponds to a thickness of approximately 55 m. The purple/pink areas representing the impedance decrease below the Keg River horizon can

be interpreted as areas where there are gas and solvent. These areas appear to correlate to some of the injection wells in the south lobe. The north lobe does not show any impedance decrease. Perhaps, this is due to the injected gas and solvent already present in the reservoir prior to 1987. Thus, additional gas and solvent would not cause a significant decrease in the impedance. A cross-section of the impedance change is shown in Figure 26. The injected gas and solvent, represented in yellow and circled in Figure 26, increased from 1987 to 2002.

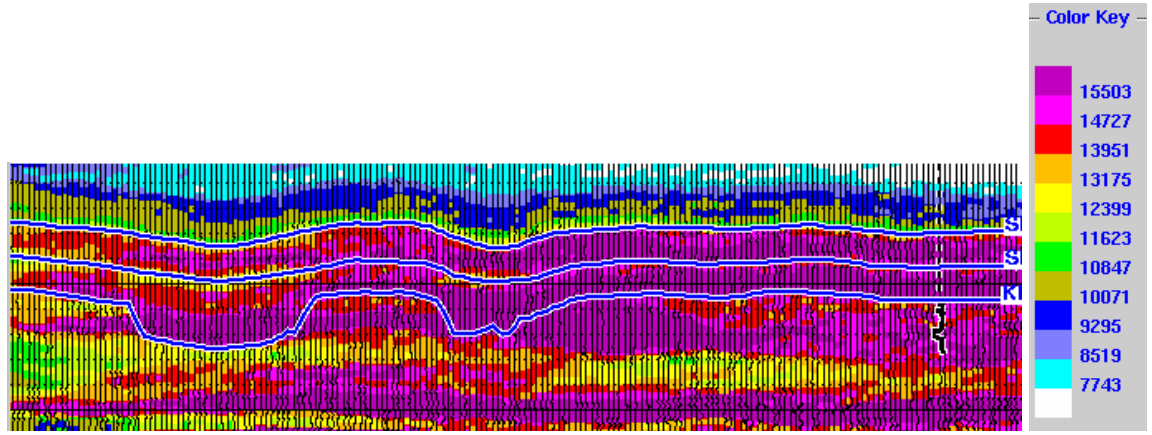

a)

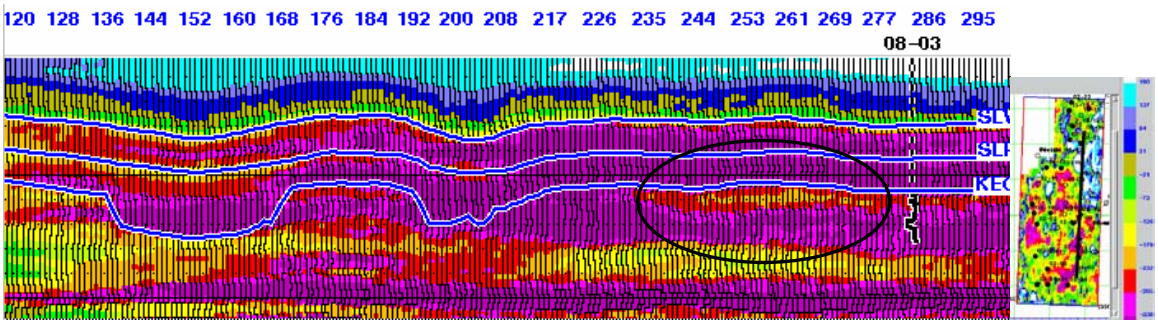

b)

Figure 26. a) 1987 impedance data; cross-line 120. b) 2002 impedance data (same cross-section) that has been time-lapse processed. Note the change of impedance in the circled zone. The presence of gas and solvent will cause a change in impedance.

Unfortunately, the impedance change map does not correlate well to the time-delay map in the north lobe, although, the results in the south lobe do correlate well. Also, the impedance change map (Figure 25) correlates well to the isochron map (Figure 15) in the south lobe but not so well in the north lobe. Based on the correlation to the isochron map, it appears that the time-delay map is slightly more robust than the impedance change map but the impedance change map is more robust than the amplitude change map.

5.5 Conclusion

The time-delay results match the location of the injection wells fairly well. They also match the shape of the reservoir. There are time-delays in the majority of the reservoir. The amplitude change results do not correlate very well to the time-delay results nor to the locations of the injection wells. The amplitude change results are also not as robust as the time-delay results. The presence of noise can greatly affect the amplitude of seismic data. Also, the amount of gas saturation may not affect the reflection amplitude at the top of the Keg River horizon, according to Domenico (1974). This means that additional gas and solvent injected will not cause an amplitude change. Also, there is already gas and solvent within the reservoir in 1987 because the 1987 survey was acquired three years after the start of gas and solvent injection. This makes it difficult to interpret the seismic data. The impedance change results are fairly good in the south lobe because the changes match the location of the injection wells but the results are poor in the north lobe. The next chapter will deal with comparing the time-delay map with the geological, engineering, and other geophysical results. The time-delay map is

used to imply the location of the gas and solvent within the reservoir but will need to be interpreted with respect to the geology.

Chapter Six: COMPARE SEISMIC RESULTS WITH OTHER RESULTS

6.1 Introduction

At each location of the reservoir, from 1987 to 2002, the porosity remained the same and the pressure also remained the same. Also, the survey from 1987 to 2002 has been time-lapse processed in order to make the surveys the same outside the production zones. Therefore, the only changes from 1987 to 2002 are due to fluid changes or possibly due to the opening of new fractures as gas and solvent were injected. The time-delay map, as opposed to the amplitude change and the impedance change map, was the map best used to infer areas where gas and solvent are present.

The Gassmann calculation is used to determine what type of changes are expected due to the injection of fluids. The calculations are then converted into time values. Thus, the time values calculated using the Gassmann equation could be compared to the seismic time-delay map. The time-delay seismic results will also be compared with the geology, which is represented by the porosity type map, and the reservoir engineer results, which are represented by the maps made using the reservoir simulation data. The time-delay results will also be compared with other maps such as the isochron map.

6.2 Compare the Gassmann calculated time-delay map with the seismic time-delay map

There are approximately 60 000 grid blocks in the reservoir simulation flow model for this reservoir. Each grid block has various values assigned to it. For example, every grid block has a porosity value. Similarly, every grid block also has a water saturation value, an oil saturation value, a gas saturation value and a solvent saturation value. These

values could be used to calculate the expected fluid changes using the Gassmann equation. The results are then converted to time values and displayed in map view. To do these calculations, we use the Gassmann equation and the Batzle and Wang (1992) derived fluid properties. More detailed calculations are found in Appendix F but the general procedure is this:

1. Find the bulk modulus and the density of water, oil, gas and solvent at each grid point using the Batzle and Wang (1992) equations. The parameters used as input to these equations are found in Table 6. Appendix G contains some useful equations to help determine the values for Table 6. The results are shown in Table 7.
2. Find the density of the combined fluids. Then find the total density of the rock.
3. Find the arithmetic and the harmonic bulk modulus of the fluids. Calculate the average of the arithmetic and the harmonic values. Find the dry bulk modulus. Then use the Gassmann equation to find the bulk modulus of a saturated rock.
4. Calculate the velocity at each grid point for both the 1987 data and the 2002 data.
5. Knowing the height of each grid block (each grid block has a different height) and the velocity of each grid block, calculate the travel time.
6. Do steps 2-5 for both the 1987 data and the 2002 data.
7. Subtract the 1987 travel time from the 2002 travel time to find the time difference.
8. Since we are comparing these results to the time-delay map, we need to add up the time differences found at each map location. Then our calculations can be plotted and observed in map view shown in Figure 27.

Table 6. Fluid input values for the Batzle & Wang (1992) calculations

Pressure (MPa)	Temperature (°C)	Gas-Oil-Ratio	Oil Gravity (API)	Gas Gravity	Solvent Gravity
17	87	79.78	39	0.683	1.13

Table 7. Fluid output values from the Batzle & Wang (1992) calculations

	Water	Oil	Gas	Solvent	Dolomite
Density ρ (g/cm^3)	0.9832	0.7279	0.1272	0.293	2.87
Bulk modulus K (GPa)	2.5005	0.6771	0.0334	0.056	94.9

The calculated time-delay map, calculated from the Gassmann equation and the Batzle and Wang (1992) derived fluid properties, can be compared to the seismic time-delay map. The Gassmann calculated time-delay map represents the engineering results and the time-delay map represents the geophysical results

On the Gassmann calculated time-delay map, there are more time changes found in the north lobe and in the northeastern/central part of the south lobe. The changes found are at an average of 0.269 ms to a maximum of 1 ms. The changes are even smaller elsewhere in the reservoir.

A side-by-side comparison of the Gassmann calculated time-delay map (Figure 27) and the seismic time-delay map (also Figure 27) shows that the time-delays are mainly similar in the north lobe. They are different because the calculated time-delay map shows a lot less change than the seismic time-delay map. This suggests that the Gassmann equation, used in the Gassmann calculated time-delay map, underpredicts the changes found in seismic data for this carbonate reservoir. This is because the low

frequency assumption of the Gassmann equation is violated. The reservoir is mostly vuggy and has some fractures, and so the velocity changes seen on seismic data are bigger than expected. The underprediction of changes is similar to the results found by Hirsche and Hirsche (1998) and Hirsche et al. (1997). As an aside, 27a) have positive values and 27b) has negative values because they are determined differently. One figure determines the changes with respect to the Base survey and one figure determines the changes with respect to the Monitor survey.

a) b)

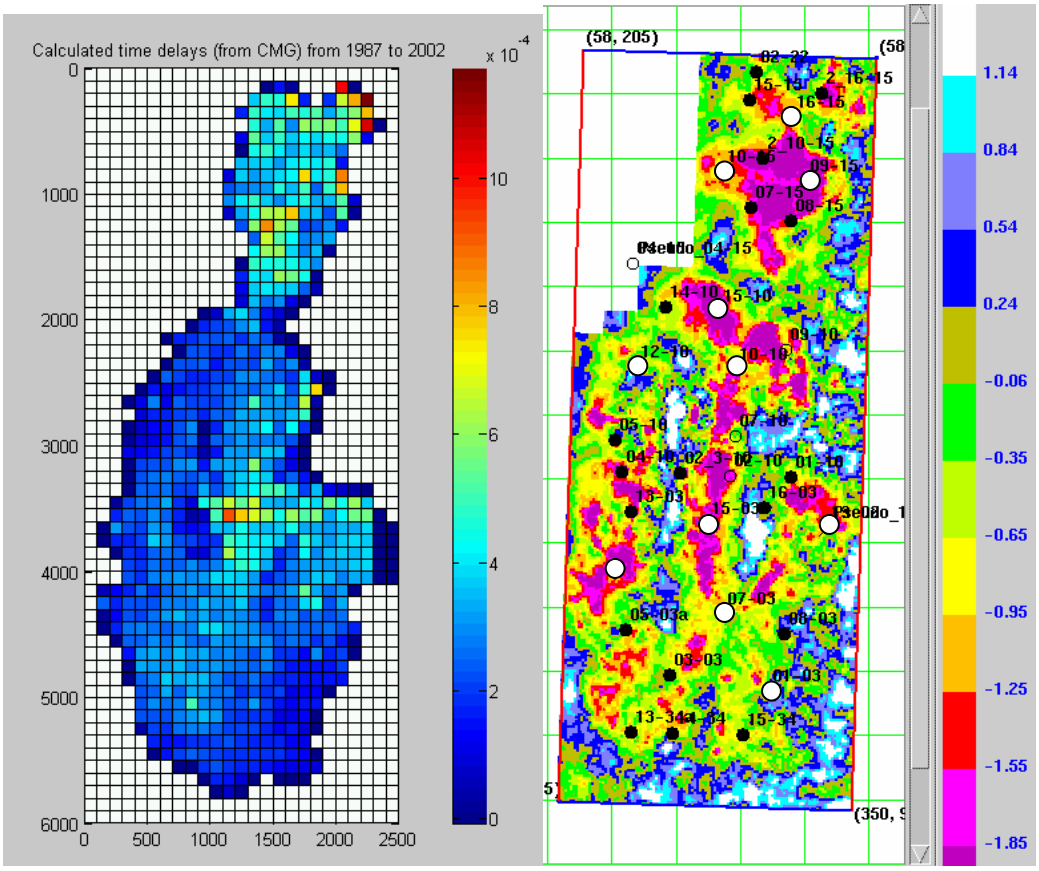

Figure 27. a) Gassmann calculated time-delay map (seconds) based on saturation and porosity results from the reservoir simulation. These results are based on calculations using the Gassmann equation and the Batzle and Wang fluid derived properties (1992). The average calculated time-delay is 0.269 ms with a standard deviation of 0.164 ms. b) Time-delay map for comparison (milliseconds).

6.2.1 Further tests

The time-delays calculated using the Gassmann equation and the Batzle and Wang (1992) equations are fairly small. The velocity changes were approximately 2%. The dry bulk modulus in this study was calculated to be at approximately 40 GPa, which is fairly high. The maximum value of K_{dry} was 46 GPa and the minimum value was 31 GPa. A test was done to see how changes in dry bulk modulus would affect the velocity changes. The dry bulk modulus was determined using the dry V_P/V_S ratio and the dry velocity measured in the laboratory on core from well 15-3 and well 15-15. If the dry bulk modulus is decreased to 30 GPa, the velocity changes increase to approximately 4%. At K_{dry} of 20GPa, the velocity changes are approximately 7% and at K_{dry} of 10 GPa, the velocity changes are approximately 14%. A general rule of thumb states that velocity changes should be more than 5% to be significant (J.Zhang, personal communications, 2003) or less than 30 GPa in this case. Perhaps one of the reasons that the dry bulk modulus is high for this study is that the results measured from core analysis are biased. The cores from well 15-3 and 15-15 may not accurately represent the whole reservoir and the reservoir is also extremely heterogeneous. Parts of the reservoir crumbled when they were being cored, and thus core were not obtained for very weak rocks. Thus, the dry bulk modulus may actually be lower than 40 GPa.

The fluid modulus values used in this study are found in Table 8. Another test was done to see how much the fluid modulus had an effect on the results. In this study, the fluid modulus was determined by taking the average of the harmonic and the arithmetic fluid modulus. It appears that whether I use only the harmonic or only the

arithmetic method to calculate the fluid modulus, the Gassmann calculated time-delay results are still very small.

Table 8. Fluid modulus values used in this study

	Average of all grid blocks (GPa)	Standard deviation (GPa)
K_{fl} arithmetic 1987	1.426	0.384
K_{fl} harmonic 1987	0.956	0.292
K_{fl} average 1987	1.191	0.334
K_{fl} arithmetic 1987	0.967	0.527
K_{fl} harmonic 2002	0.582	0.463
K_{fl} average 2002	0.774	0.490

6.2.2 Comment on modelling

Modelling using the Pro4D software was attempted to estimate the amount of change that would be expected if fluid were injected into the reservoir. The well logs were converted to synthetic seismograms and then time-lapse analysis was applied to the synthetic seismograms. Unfortunately, the time-delays extracted from modelling were very small. Modelling with well 12-10 and well 7-15, time-delays were approximately –0.3 ms, which is barely any change. The time-delays from modelling are small because the Gassmann equation was used and the Gassmann equation appears to underpredict the seismic changes. Thus, modelling did not work very well in this reservoir.

Also, the reservoir is very heterogeneous, both vertically and horizontally. The sonic well logs and the density well logs varied from well to well. Thus, modelling with certain wells would give estimates of certain time-delays but modelling with other wells would give different results. For example, modelling with well 10-10 showed changes of –1 ms, which is still very small but the changes are also different than with well 12-10 and well 7-15. Modelling is usually used to predict changes and then the results are

compared to real seismic data. But it is difficult to compare modelling to real seismic data when the modelling from well to well gave different results.

6.3 Compare the isochron map with the time-delay map

a) b)

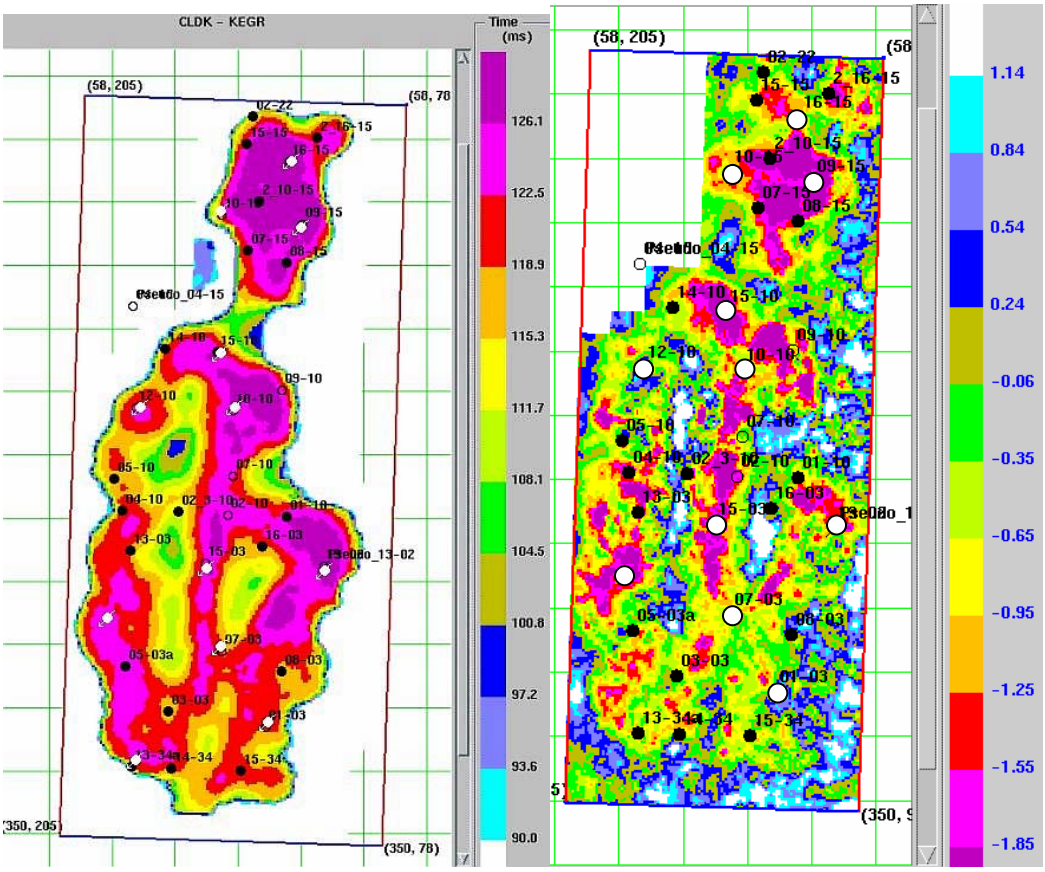

Figure 28. a) Isochron map of the Keg River horizon to the Cold Lake horizon (milliseconds). The map represents the thickness of the reservoir. b) Time-delay map for comparison (milliseconds)

The isochron map, of the Keg River horizon to the Cold Lake horizon, indirectly represents the thickness of the reservoir. The time-delay map is very similar in shape to the isochron map (Figure 28). The injected fluids could be interpreted to be in the

locations where the time-delays are coloured pink/purple. Note that the injection wells (coloured white dots) correspond to the perceived injected fluids found in the time-delay map.

6.3.1 Comment on show maps

Show maps with the injection history are shown in Figure 29. The size of the bubbles represents the amount of fluids injected. Although fluids are injected, a lot of fluids are also produced. One-third to one-half of the injected fluids get produced (L.Carr, personal communications, 2003). Also, when the fluids are injected below the subsurface, they tend to move around within the reservoir. Therefore, show maps are not too useful in this project.

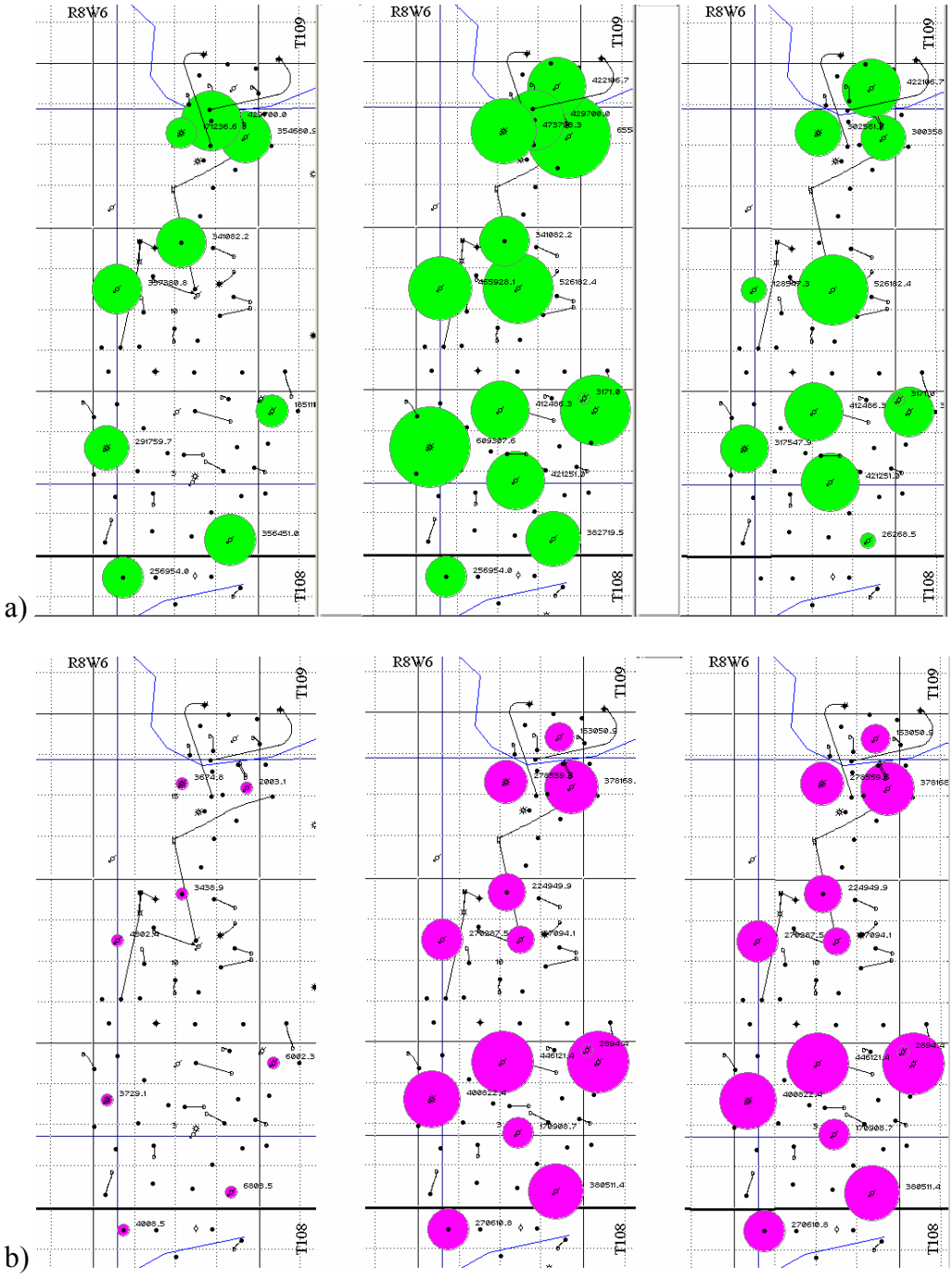

Figure 29. a) Show map represents the amount of solvent injected in 1987 , 2002, and the difference between 1987 and 2002, respectively. b) Show map represents the amount of gas injected in 1987 , 2002, and the difference between 1987 and 2002, respectively. The bigger the bubble size, the more injected gas and solvent.

6.4 Compare the fluid thickness map (engineering results) with the time-delay map

Figure 30a shows a map of the thickness difference from 1987 to 2002 of the solvent plus gas amount. This map represents the change in thickness of gas plus solvent calculated from the reservoir simulation. These are the results that the engineers have at this point of the simulation. The north lobe and the northeastern south lobe contain 50 m increase in the thickness of gas plus solvent. Elsewhere in the reservoir, the gas plus solvent thickness increase is approximately 30 m. The shape of this map resembles the isochron map.

Now we can compare this map to the time-delay map (also in Figure 30). The geophysical time-lapse results and the results from the reservoir simulation have similarities and differences. Again, the north lobe and the northeastern part of the south lobe show big changes in both maps. But, the change is greater on the western side of the reservoir in the time-delay map. Note that at well 12-10, located in the northwest corner of the south lobe, the time-delay map shows very little change compared to the engineering map. There are a few other places where the simulation results show locations of injected gas but the seismic data do not. Nevertheless, the results are generally similar.

a) b)

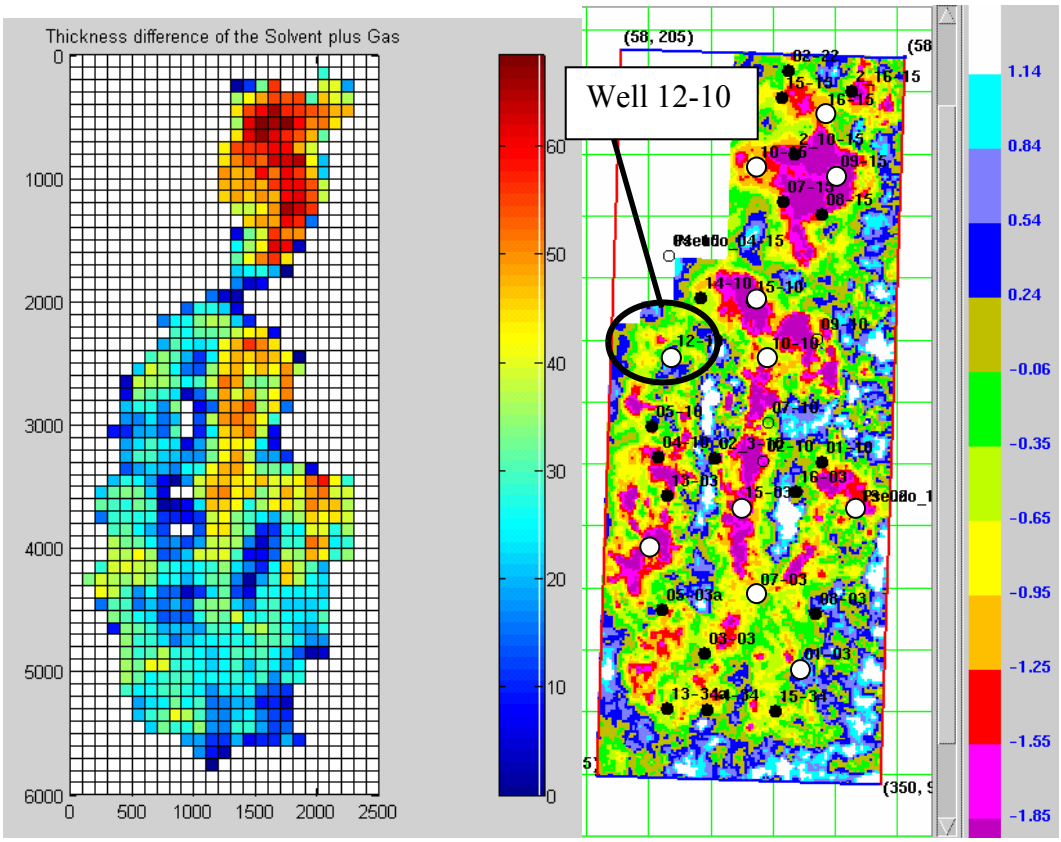

Figure 30. a) Difference of gas and solvent thickness between 1987 and 2002 (metres). b) Time-delay map for comparison (milliseconds).

6.4.1 Crossplot of the fluid thickness map at well locations with the time-delay map

The engineering map in Figure 30 was taken from the reservoir simulation. These results cover the whole map area of the reservoir. Unfortunately, most of the data are taken from well locations and interpolated in order to get the information in between the wells. This next map (Figure 31) only shows the thickness found at the well locations. Although the map is colour-coded, it is still very difficult to compare to the time-delay

map. Thus, a crossplot (Figure 32) is made between the engineering data and the seismic time-delay map.

The correlation between the two data set is approximately 0.17, which is not too high. One reason why the correlation is weak is that the porosity type is not taken into consideration. The next section will interpret the time-delay map with respect to the porosity type map.

a) b)

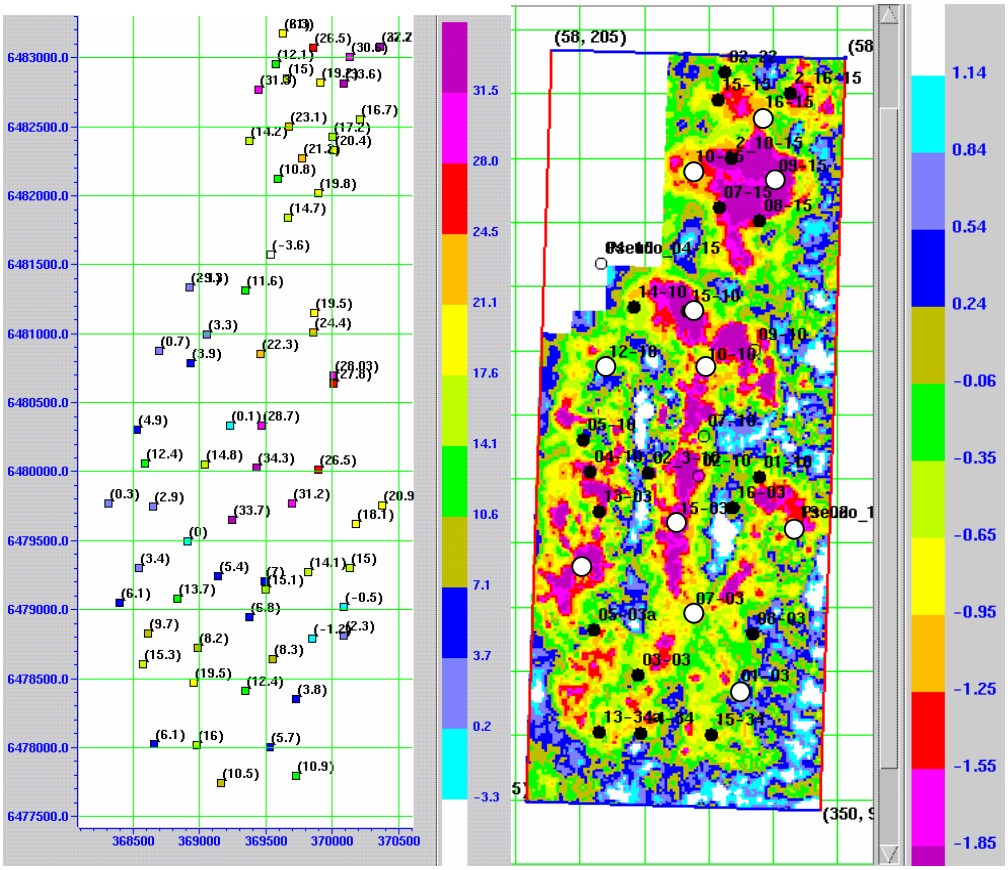

Figure 31. a) Difference of gas and solvent thickness map only at well locations between 1987 and 2002 (metres). b) Time-delay map for comparison (milliseconds).

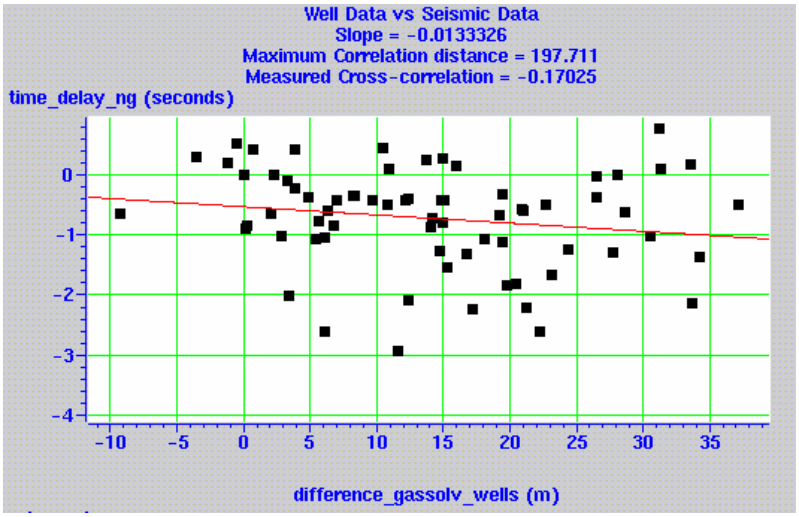

Figure 32. Crossplot of the gas and solvent thickness map at well locations versus the time-delay map. There is a weak correlation.

6.5 Compare the porosity type map with the time-delay map

The porosity and the porosity type vary both vertically and horizontally within the reservoir. The porosity type has been averaged vertically and displayed in map view in order to be compared to the time-delay map. The porosity type map (Figure 33) shows that the edges of the reef are mostly vuggy and the north-west corner of the south lobe has a zone that is mostly intergranular. There does not appear to be any time-delay at well 12-10. But, well 12-10 is believed to contain a high amount of injected gas and solvent even though the time-delay map does not indicate this situation (L. Carr, personal communication, 2003). This may be related to the porosity type, which is intergranular and has a high pore aspect ratio. An area that has a high pore aspect ratio does not show very much velocity change. Thus, we can conclude that although a zone may have a porosity type which is intergranular and may lack a time-delay, this does not mean there is no gas and solvent saturation, nor is there necessarily bypassed oil.

a) b)

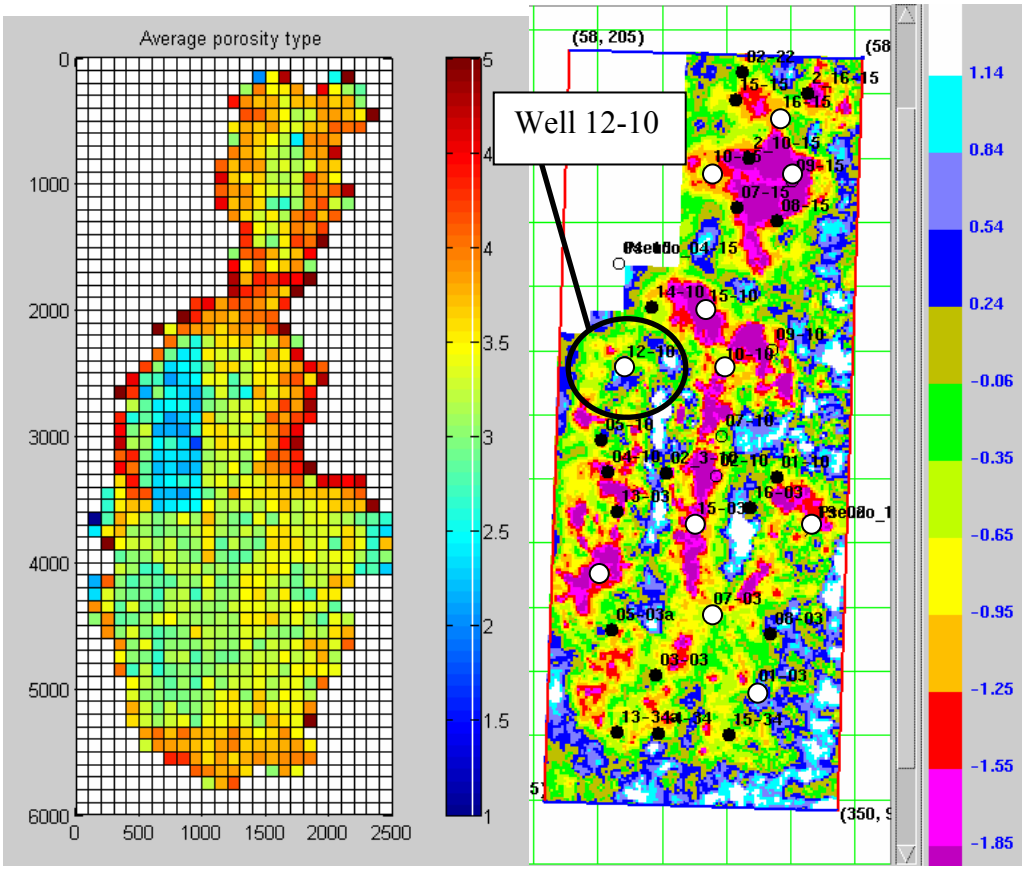

Figure 33. a) Average porosity type map b) Time-delay map for comparison (milliseconds)

LEGEND for porosity type map
Porosity type 5: mostly large vugs
Porosity type 4: medium vugs
Porosity type 3: Predominantly vuggy with secondary intergranular matrix
Porosity type 2: Predominantly intergranular with reservoir quality porosity
Porosity type 1: Entirely intergranular with downgraded porosity

According to the time-delay map, there are relatively large time-delays within certain zones of the reservoir. One might say that those zones will have more gas and solvent present. Unfortunately, the porosity and the porosity type will influence the time-delay results. Thus, the magnitude of time-delay would not necessarily be proportional to

the amount of solvent and gas injected. For example, the time-delay through a vuggy porosity type area is different than the time-delay through an intergranular porosity type area even though there may be the same amount of gas and solvent present. Time-delays or velocity changes are only detected in areas of certain porosity types. Thus, the magnitude of the time-delay does not necessarily indicate the amount of gas and solvent present.

Overall, the time-delay results help predict gas and solvent in only some but not all locations of the reservoir. This is because the reservoir is very hetereogeneous and changes can only be detected in some porosity types. We can interpret vuggy type zones with more confidence than the intergranular type zones.

6.6 Conclusions

The Gassmann equation is used to predict what kind of bulk modulus change that can be expected with a change of fluid. Unfortunately, the Gassmann equation underpredicts the velocity change because the low frequency assumption is violated in this pool, and thus the pore pressure does not have time to equilibrate. The calculated map made using the Gassmann equation shows less of a time-delay than the seismic time-delay map. The time-delay map does compare very well to the isochron map and to the engineering map. But it is very important to interpret the time-delay map with respect to the porosity type because the pore geometry has a big effect on the time-delay results. Since the porosity type varies drastically within the reservoir, it becomes difficult to interpret the time-delay map. However, we can conclude that areas where there are time-delays have gas and solvent present. This is because the porosity and the pressure remain the same from one survey to the next and so the seismic changes are due to the presence

of the injected fluids. Also, the magnitude of time-delay is not proportional to the amount of gas and solvent in the reservoir because of the pore geometry effect. Unfortunately, we cannot interpret areas where there are no time-delays because the porosity type may prevent gas and solvent from being detected. Also, it is hard to interpret the results due to the presence of injected gas and solvent prior to the first survey. This study, therefore, cannot be used to detect bypassed oil and gas.

Chapter Seven: CONCLUSIONS

7.1 Limitations of study

Time-lapse analysis is useful because it obtains information in between the wells. However, there are some limitations to this study. First of all, the Base survey should have been acquired prior to tertiary production. Rather, it was acquired three years after gas and solvent have already been injected. Therefore, it is harder to interpret the results of the locations of where the gas and the solvent are suspected to be in the reservoir. Secondly, the zone of interest is poor in frequency content and thus the resolution is low. This makes the amplitude results difficult to interpret. Thirdly, the surrounding seismic traces around the pool have been removed. This makes it harder to confirm that the differences within the pool are correct compared with the differences around the pool. However, the lack of time differences above the reservoir can be used to justify the time-differences within the reservoir. Lastly, carbonate reservoirs are usually thought to be unsuitable candidates for time-lapse analysis because the changes are small. The time-delays found in this study were less than 2 ms, which is the sampling interval. However, a test was performed to check whether there were time-delays outside the production zone and there were none. Also, the time-delay results were anomalous despite the limitations of this study.

7.2 Conclusions

1. The presence of gas and solvent were best interpreted using the time-delay map. The porosity in the Rainbow B pool is very heterogeneous and so the time-delay map had to be interpreted with respect to the porosity. The factor that most

affects fluid related seismic changes is the pore type. The changes are greater for a rock with flat low aspect ratio pores than for a rock with round high aspect ratio pores. Similarly, an area of the reservoir with vuggy type porosity, which behaves similar to rocks with low aspect ratio pores, is more sensitive to fluid saturation than an area with intergranular type porosity. In fact, there were no time-delays at well 12-10, which is an intergranular type porosity area, even though the engineers know that there is gas and solvent present. It appears that time delays are visible at locations where the porosity type is vuggy but not visible at locations where the porosity type is intergranular. Where there are time-delays, regardless of the magnitude of the time-delays, that area is interpreted with having the presence of gas and solvent. Where there are no time-delays, that area may have an intergranular porosity type and so changes are not detectable. Thus, we could not interpret bypassed oil in this study. Also, there may not be any time-delay detected if there already was a thick bank of gas and solvent in the reservoir prior to the first survey. Smaller amounts of fluid injected may not cause much difference to the time-delays. We can be more confident of our interpretation in areas where the porosity type is vuggy and where the pore aspect ratio is low because reservoir fluid changes will show up on the time-delay map. Time-lapse analysis for this study is useful in confirming the presence of gas and solvent with the reservoir simulation but is not useful in detecting bypassed oil.

2. The amplitude change results do not appear as reliable as the time-delay results. However, the impedance change results correlate better to the injection wells than the amplitude change results. There may not be any amplitude changes detected

if there already were gas and solvent in the reservoir prior to the first survey. This is because the presence of 5% gas saturation and the presence of 100% gas saturation can display the same reflection amplitude. Thus, any additional gas and solvent would not cause any significant reflection amplitude change. Also, the amplitude change data and the impedance change data do not match the geology and the engineering data as well as the time-delay data.

3. The Gassmann analysis underpredicts changes due to solvent and gas injection as Hirsche and Hirsche (1998) and Hirsche et al. (1997) have also shown. The time-delays found in this study are fairly low, at approximately 2 ms, but are still much higher than the changes the Gassmann analysis predicts. Although the changes found on the time-delay map are small, they are still useful and anomalous in interpreting the production related changes.
4. The reservoir appears mostly flooded. According to the time-delay map, there is gas and solvent at the saddle point, the area in between the north and the south lobe. The time-lapse data matches the injection well, isochron map and the engineering fluid thickness data fairly well.

Time-lapse analysis is not commonly done for carbonate reservoirs but this case study showed fluid changes that were bigger than expected. With the increasing use of enhanced oil recovery methods, the use of time-lapse analysis could also increase. Overall, time-lapse analysis seems to work better and for more case studies than we expect (I.Jack, personal communication, 2003). Given positive results, time-lapse may be useful in carbonate reservoirs, especially with the improved seismic resolution possible since 1987.

REFERENCES

Batzle, M., Wang, Z., 1992, Seismic properties of pore fluids: Geophysics, **57**, 1396-1408.

Brown, L.T., Davis, T.L., Batzle, M., 2002, Integration of rock physics, reservoir simulation, and time-lapse seismic data for reservoir characterization at Weyburn Field, Saskatchewan: 72nd Ann. Internat. Mtg., Soc. Expl. Geophys., Expanded Abstracts, 1708-1711.

Davis, T.L., Terrell, M.J., Benson, R.D., Cardona, R., Kendall, R.R., Winarsky, R., 2003, Multicomponent seismic characterization and monitoring of the CO_2 flood at Weyburn Field, Saskatchewan: The Leading Edge, **22**, 696-697.

Domenico, S.N., 1974, Effect of water saturation on seismic reflectivity of sand reservoirs encased in shale: Geophysics, **39**, 759-769.

Eberli, G.P., Baechle, G.T., Anselmetti, F.S., Incze, M.L., 2003, Factors controlling elastic properties in carbonate sediments and rocks: The Leading Edge, **22**, 654-660.

Fong, D.K., Wong, F.Y., Nagel, R.G., Peggs, J.K., 1991, Combining a volumetric model with a pseudo-miscible field simulation to achieve uniform fluid levelling in the Rainbow Keg River "B" Pool: Journal of Canadian Petroleum Technology, **30**, 65-76.

Gassmann, F., 1951, Uber die elastizität poröser medien: Vier. der Natur. Gesellschaft in Zürich, **96**, 1-23.

Greaves, R.J., and Fulp, T.J., 1987, Three-dimensional seismic monitoring of an enhanced oil recovery process: Geophysics, **52**, 1175-1187.

Hirsche, K., 2002, Heavy Oil Workshop: unpublished course notes for Hampson-Russell Partnership Ltd.

Hirsche, K., Hirsche, J., 1998, Seismic monitoring of gas injection and solvent floods in carbonate reservoirs: unpublished internal report for Western Geophysical.

Hirsche, K., Batzle, M., Knight, R., Wang, Z., Mewhort, L., Davis, R., and Sedgwick, G., 1997, Seismic monitoring of gas floods in carbonate reservoirs: From rock physics to field testing: 67th Ann. Internat. Mtg., Soc. Expl. Geophys., Expanded Abstracts, 902-905.

Jack, I., 1998, Time-lapse seismic in reservoir management, Distinguished Instructor Short Course: Society of Exploration Geophysicists.

Jenkins, S.D., Waite, M.W., Bee, M.F., 1997, Time-lapse monitoring of the Duri steamflood: A pilot and case study: The Leading Edge, **16**, 1267 – 1273.

Li, G., 2003, 4D seismic monitoring of CO[sub 2] flood in a thin fractured carbonate reservoir: The Leading Edge, **22**, 690-695.

Kuster**,** G.T., Toksöz, M.N., 1974, Velocity and attenuation of seismic waves in two-phase media: Part 1. theoretical formulations: Geophysics, **39**, 587-606.

Laflamme, A.K., 1993, "B" pool reservoir characterization pilot study (section d): Carbonate Technical Group Geological Report: unpublished internal report for Husky Energy Inc.

Landro, M., Veire, H.H., Duffaut, K., Najjar, N., 2003, Discrimination between pressure and fluid saturation changes from marine multicomponent time-lapse seismic data: Geophysics, **68**, 1592-1599.

Landro, M., 2001, Discrimination between pressure and fluid saturation changes from time-lapse seismic data: Geophysics, **66**, 836-844.

Lumley, D.E., 2001a, The next wave in reservoir monitoring: The instrumented oil field: The Leading Edge, **20**, 640-648.

Lumley, D.E., 2001b, Time-lapse seismic reservoir monitoring: Geophysics, **66**, 50-53.

Lumley, D.E., Behrens, R.A., Wang, Z., 1997, Assessing the technical risk of a 4D seismic project: The Leading Edge, **16**, 1287-1291.

Mavko, G., Mukerji, T., Dvorkin, J., 1998, The rock physics handbook – Tools for seismic analysis in porous media: Cambridge Univ. Press.

Meadows, M., 2001, Enhancements to Landro's method for separating time-lapse pressure and saturation changes: 71st Ann. Internat. Mtg., Soc. Expl. Geophys., Expanded Abstracts, 1652-1655.

Nagel, R.G., Hunter, B.E., Peggs, J.K., Fong, D.K., Mazzocchi, E., 1990, Tertiary application of a hydrocarbon miscible pool: Rainbow Keg River "B" pool: SPE Reservoir Engineering, 301-378.

Rickett, J.E., Lumley, D.E., 2001, Crossequalization data processing for time-lapse seismic reservoir monitoring: A case study from the Gulf of Mexico: Geophysics, **66**, 1015-1025.

Ross, C.P., Altan, M.S., 1997, Time-lapse seismic monitoring: Some shortcomings in nonuniform processing: The Leading Edge, **16**, 931-937.

Ross, C.P., Cunningham, G.B., Weber, D.P., 1996, Inside the crossequalization black box: The Leading Edge, **15**, 1233-1240.

Smith, T.M., Sondergeld, C.H., Rai, C.S., 2003, Gassmann fluid substitutions: a tutorial: Geophysics, **68**, 430-440.

Talley, D.J., Davis, T.L., Benson, R.D., and Roche, S.L., 1998, Dynamic reservoir characterization of Vacuum Field: The Leading Edge, **17**, 1396-1402.

Terrell, M.J., Davis, T.L., Brown, L., Fuck, R., 2002, Seismic monitoring of a CO_2 flood at Weyburn field, Saskatchewan, Canada: demonstrating the robustness of time-lapse seismology: 72nd Ann. Inter. Mtg., Soc. Expl. Geophys., Expanded Abstracts, 1673-1676.

Waite, M.W., Sigit, R., 1997, Seismic monitoring of the Duri steamflood: Application to reservoir management: The Leading Edge, **16**, 1275 – 1278.

Wang, Z., 2001, Fundamentals of seismic rock physics: Geophysics, **66**, 398-412.

Wang, Z., Cates, M.E., Langan, R.T., 1998, Seismic monitoring of a CO_2 flood in a carbonate reservoir: A rock physics study: Geophysics, **63**, 1604 – 1617.

Wang, Z., 1997, Feasibility of time-lapse seismic reservoir monitoring: The physical basis: The Leading Edge, **16**, 1327 – 1329.

Wang, Z., Nur, A., 1990, Wave velocities in hydrocarbon-saturated rocks: Experimental results: Geophysics, **55,** 723-733.

Yilmaz, O, 1987, Seismic Data Processing: Society of Exploration Geophysicists.

APPENDIX A: Batzle and Wang Equations (1992)

Some of the equations from the Batzle and Wang (1992) paper are below. These equations can be used to determine the density and the bulk modulus of gas, oil, and brine. The fluid properties are based on pressure and temperature conditions as well as the composition of the fluids.

Gas

$$\rho_g \cong \frac{28.8GP}{ZRT_a} \tag{1}$$

$$Z = [0.03 + 0.00527(3.5 - T_{pr})^3]P_{pr} + (0.642T_{pr} - 0.007T_{pr}{}^4 - 0.52) + E \tag{2}$$

$$E = 0.109(3.85 - T_{pr})^2 \exp\{-[0.45 + 8(0.56 - 1/T_{pr})^2]P_{pr}{}^{1.2}/T_{pr}\} \tag{3}$$

$$P_{pr} = P/(4.892 - 0.4048G) \tag{4}$$

$$T_{pr} = T_a/(94.72 + 170.75G) \tag{5}$$

$$K_g = \frac{\gamma P}{\left(1 - \frac{P_{pr}}{Z}\frac{\partial Z}{\partial P_{pr}}\right)} \tag{6}$$

$$T_a = T + 273.15 \tag{7}$$

$$\gamma = 0.85 + \frac{5.6}{P_{pr} + 2} + \frac{27.1}{(P_{pr} + 3.5)^2} - 8.7e^{-0.65(P_{pr}+1)} \tag{8}$$

where T is the temperature in degrees Celsius, T_a is the absolute temperature, P_{pr} is the pseudotemperature, T_{pr} is the pseudotemperature, P is the pressure in units of MPa, K_g is the adiabatic bulk modulus in MPa, G is the gravity where the values range from 0.45 for methane to 1.8 for gases with a higher carbon number, ρ_g is the density of gas in g/cm^3, and R is the gas constant, which is 8.31441 L kPa/(K mol).

Oil

$$\rho = \rho_P / [0.972 + 3.81 * 10^{-4} (T + 17.78)^{1.175}] \quad (9)$$

$$\rho_P = \rho_o + (0.00277P - 1.71 * 10^{-7} P^3)(\rho_o - 1.15)^2 + 3.49 * 10^{-4} P \quad (10)$$

$$V_P(m/s) = 2{,}096\left(\frac{\rho_o}{2.6 - \rho_o}\right)^{1/2} - 3.7T + 4.64P + 0.0115[4.12(1.08\rho_o^{-1} - 1)^{1/2} - 1]TP \quad (11)$$

$$API = \frac{141.5}{\rho_o} - 131.5 \quad (12)$$

where ρ is the calculated density of oil in g/cm^3, ρ_P is the density at a given pressure P (in units of MPa), T is the temperature, V_P is the velocity of dead oil, ρ_o is the density of oil at a given API, and API is the API gravity where a value of 5 is for very heavy oils and a value of 100 is for light condensates. For the velocity of live oil, please refer to Batzle and Wang (1992).

Brine

$$\rho_B = \rho_w + S\{0.668 + 0.44S + 10^{-6}[300P - 2400PS + T(80 + 3T - 3300S - 13P + 47PS)]\} \quad (13)$$

$$V_B = V_w + S(1170 - 9.6T + 0.055T^2 - 8.5 * 10^{-5} T^3 + 2.6P - 0.0029TP - 0.0476P^2) + S^{1.5}(780 - 10P + 0.16P^2) - 1820S^2 \quad (14)$$

$$K_w = \rho {V_B}^2 \quad (15)$$

where S is the salinity of a sodium chloride solution in parts per million divided by 10^6, P is the pressure in MPa, T is the temperature in degrees Celsius, and ρ_B is the density of brine in g/cm^3, ρ_W is the density of water, and V_B is the velocity of brine. For the velocity of water, V_W, please refer to Batzle and Wang (1992).

APPENDIX B: Photographs of core from well 7-10

Figure B-1. intergranular porosity

Figure B-2. mesovug porosity

Figure B-3. zebroidal porosity

Figure B-4. vuggy porosity depicted in the centre of the photograph

Figure B-5. fractured porosity

Figure B-6. porosity variation within core

APPENDIX C: How to calculate weighted averages

It is sometimes necessary to do a weighted average to take into account the importance of various terms. For example, in the Rainbow B reservoir simulation results, each grid point is a different size. An average porosity along the vertical axis is taken at each location. But, since each grid point is a different size, a weighted average would be more accurate. A weighted average could be done for the porosity with respect to the size of the grid blocks, with bigger grid blocks being weighted higher.

Table C. Example table to use to calculate the weighted average

	A	B (weights)	Product
1	25	6	150
2	40	3	120
3	50	1	50
Sum	115	10	320

Average of column A is 115 / 3 = 38.3

Weighted average of column A, with respect to column B, is 320/10 = 32

To determine the weighted average in Excel worksheets, use this equation:

= sumproduct(B1:B3, A1:A3) / sum(B1:B3)

APPENDIX D: Acquisition parameters for the Rainbow B 3D seismic data

	Rainbow B pool 1987 3D	Rainbow B pool 2002 3D
Acquisition company	Western Geophysical Party 360	Veritas Geophysical Party #3
Instruments		
Instrument make/model	Sercel 368	I/O System 2
Sample rate	2 ms	2 ms
Record length	3 seconds	4 seconds
Low cut filter/filter	Out to 178 Hz	3.75 Hz minimum phase
Notch	Out	Out
Format	SEG-D (CODE 15)	SEG-D IEEE
Source		
Source type	Dynamite	Dynamite
Charge	1 * 1 kg	2 * 1 kg
Depth	15 m	9 meters each hole
Holes	1	2 spaced at 15 meters
Receivers		
Geophones	LRS1011	OYO GS-30CT
Frequency	14 Hz	10 Hz
Damping	70 %	70 %
Number/group	9	6
Spacing	3.125 m	5 m
Group length	25 m	25 m
Spread		
Group interval	80 m	60 m
Shot point interval	80 m	60 m
Patch size	8 lines * 30 groups (240 channels live)	16 lines * 53 groups (848 channels max)
Shot line interval	400 m	400 m
Receiver line interval	220 m	220 m

In-line fold = Receiver line length / 2 / source line interval
Cross-line fold = number of receiver lines / 2
Total fold ≈ In-line fold * Cross-line fold

1987 fold ≈ 12
2002 fold ≈ 32

APPENDIX E: Time-delay and amplitude change maps with different time-lapse processing method

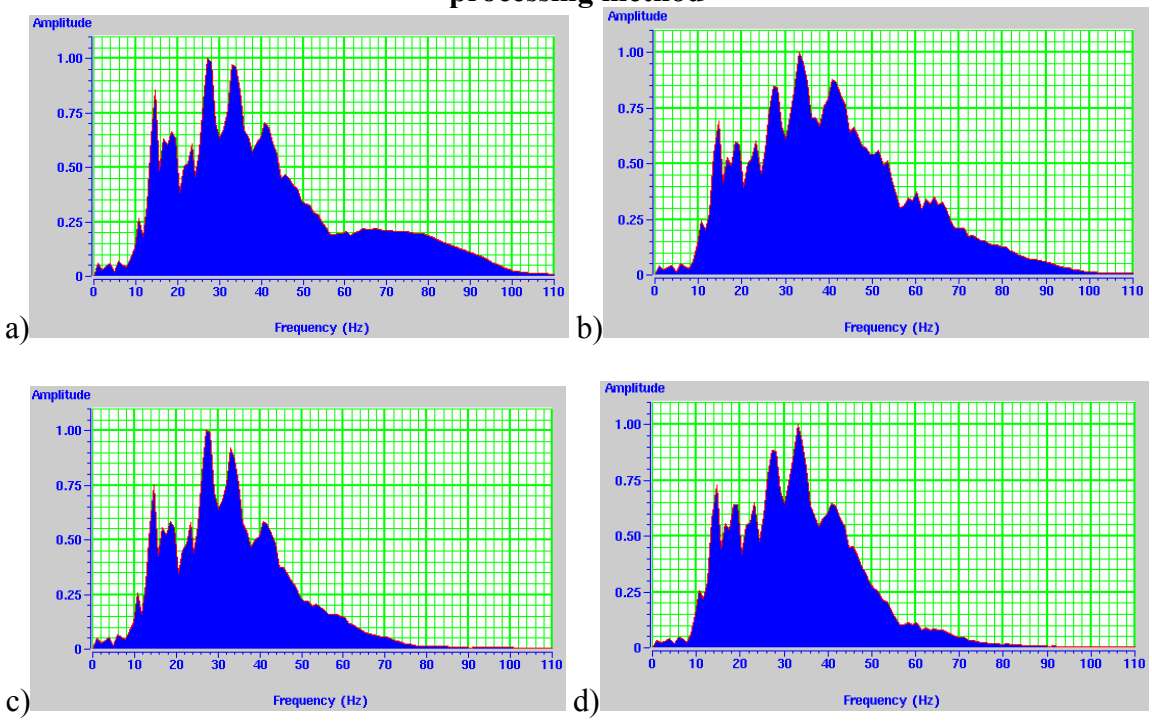

Figure E-1. a) Amplitude spectrum of the 1987 data from 750-1400 ms. b) Amplitude spectrum of the 2002 data from 750-1400 ms. c) Amplitude spectrum of the 1987 data after the shaping filter was applied from 750-1400 ms. d) Amplitude spectrum of the 2002 data after the shaping filter was applied from 750-1400 ms.

The objective of time-lapse processing is to match one survey to another survey. Unfortunately, the application of a shaping filter appears to cut down on the frequency of the seismic data. Figure E-1a and Figure E-1b show the 1987 and the 2002 amplitude spectrum, respectively. In Figure E-1c and E-1d, the 1987 and the 2002 amplitude spectrum is shown after the shaping filter is applied to the data. It appears that much of the frequency content above 70 Hz has been filtered out of the seismic data with the application of a shaping filter. The shaping filter appears to be quite harsh. Thus, the data was time-lapse processed without the application of the shaping filter to determine whether the shaping filter had any effect on the time-lapse results.

Figure E-2 shows the time-delay map and the amplitude maps with all the time-lapse processing steps applied. Figure E-3 shows the same maps without the application of a shaping filter. The time-delay maps look very similar (Figure E-2a and Figure E-3a) but the amplitude maps are slightly different. The shaping filter only changed the magnitude of the time-delay results but did not change the location of the time-delays. For example, the time-delay would only change from –2.28 ms to –1.85 ms with the application of a shaping filter. The shaping filter appears to decrease the amplitude of the 2002 data with the application of a shaping filter (compare Figure E-2d and Figure E-3d). For example, the magnitude of the amplitude difference changed from 83% to 60%. This is because the role of the shaping filter is to match the amplitude and also the static time shift, the phase, and the frequency content between the surveys. Although the shaping filter diminished the amplitude change results and the frequency content of the 2002 dataset, the location of the amplitude change remained the same.

I also tried another method of time-lapse processing where the 1987 dataset was time-lapse processed to match the 2002 dataset rather than the 2002 dataset time-lapse processed to match the 1987 dataset. This method was done to determine whether the time-lapse results could be improved. Figure E-4 and E-5 are the results with a shaping filter and without a shaping filter applied, respectively. These results are similar to the results in Figure E-2 and E-3.

Overall, whether or not a shaping filter was applied or whether or not the 2002 dataset was time-lapse processed to match the 1987 dataset, the results are similar because the time-delay and the amplitude change results remained in the same location but the magnitude of change are slightly different. The time-lapse processing method

presented in this study is where a shaping filter was applied and the 2002 dataset was time-lapse processed to match the 1987 dataset.

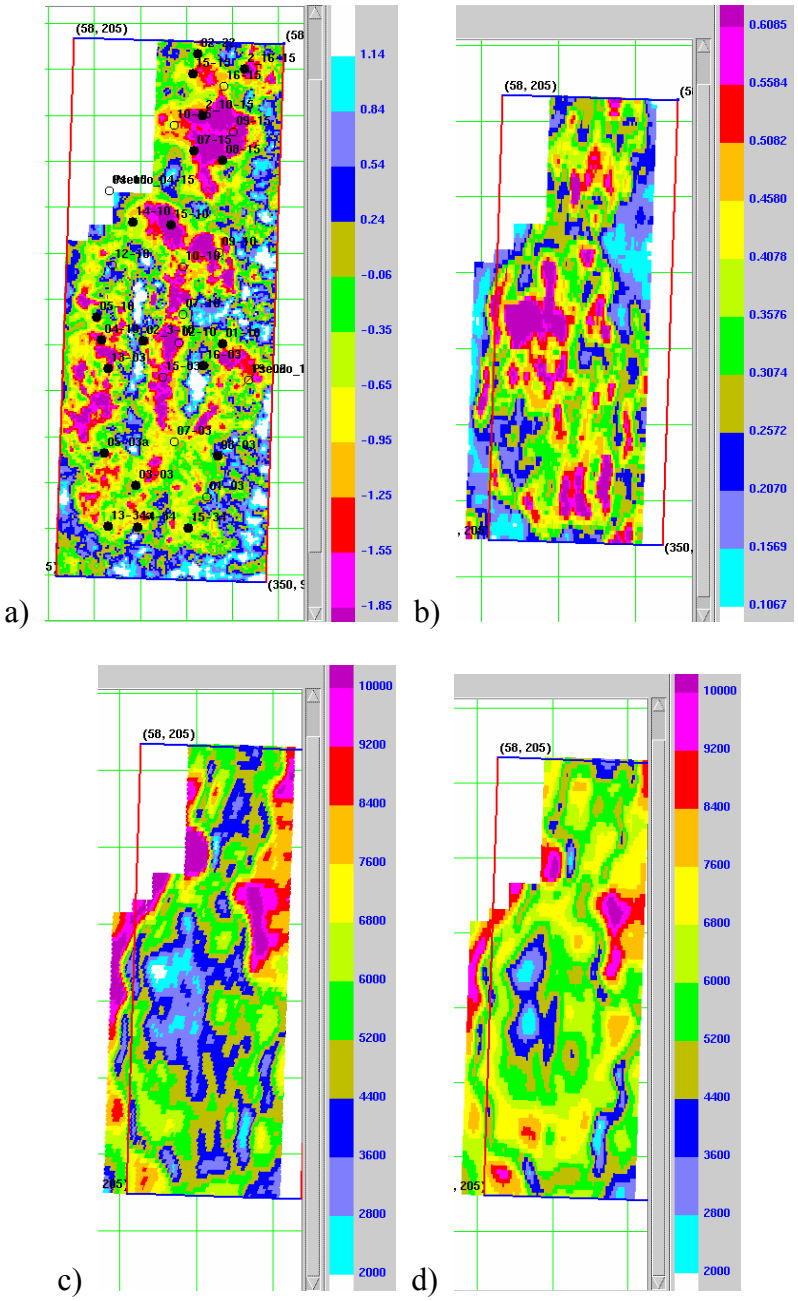

Figure E-2. a) Time-delay map (milliseconds). The 2002 survey was time-lapse processed (steps 1,2,3,4) to match the 1987 survey. b) normalized rms amplitude difference map between 1987 and 2002 (steps 1,2,3,4,5) c) 1987 rms amplitude map d) time-lapse processed 2002 rms amplitude map

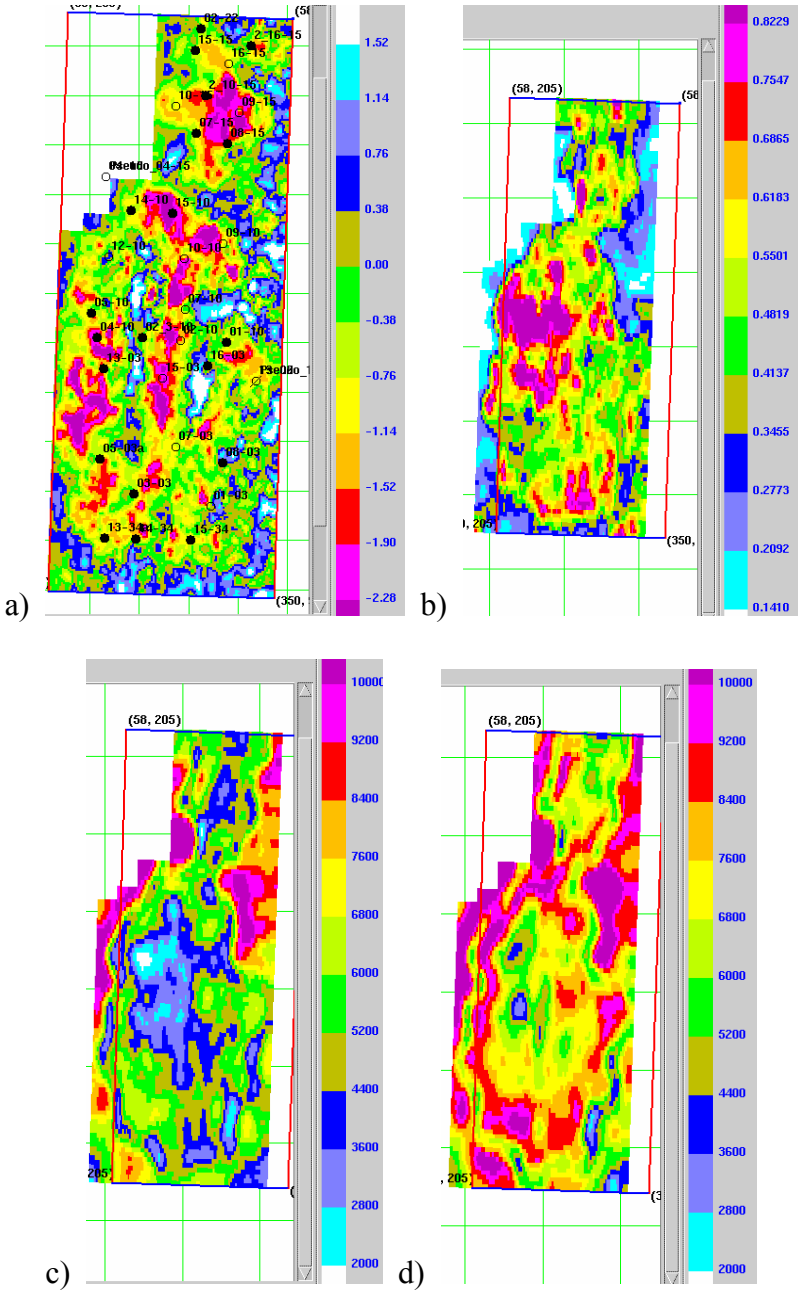

Figure E-3. a) Time-delay map (milliseconds). The 2002 survey was time-lapse processed without applying a shaping filter (steps 1,2,4) to match the 1987 survey. b) normalized rms amplitude difference map between 1987 and 2002 (steps 1,2,4,5) c) 1987 rms amplitude map d) time-lapse processed 2002 rms amplitude map

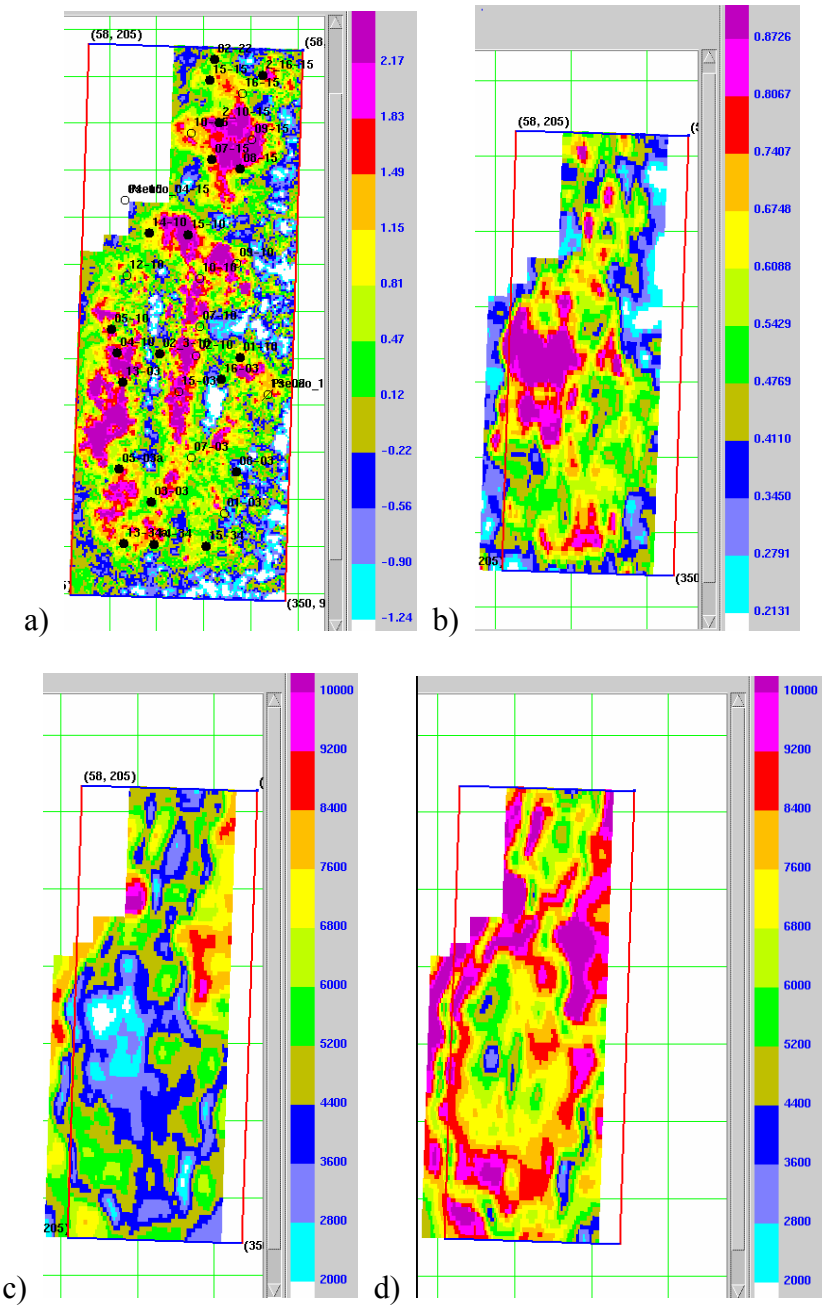

Figure E-4. a) Time-delay map (milliseconds). The 1987 survey was time-lapse processed (steps 1,2,3,4) to match the 2002 survey. b) normalized rms amplitude difference map between 1987 and 2002 (steps 1,2,3,4,5) c) time-lapse processed 1987 rms amplitude map d) 2002 rms amplitude map

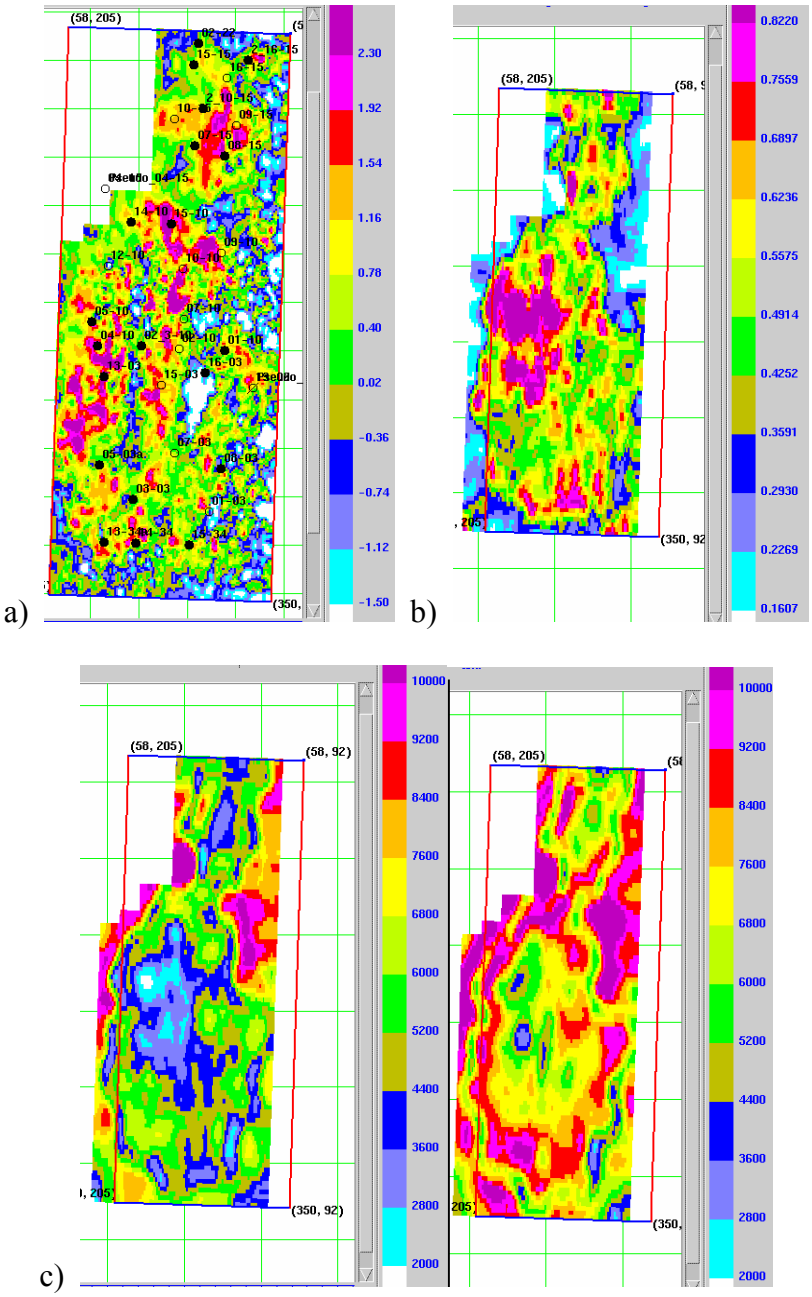

Figure E-5. a) Time-delay map (milliseconds). The 1987 survey was time-lapse processed without applying a shaping filter (steps 1,2,4) to match the 2002 survey. b) normalized rms amplitude difference map between 1987 and 2002 (steps 1,2,4,5) c) time-lapse processed 1987 rms amplitude map d) 2002 rms amplitude map

Time-lapse processing steps:

1. Regridding
2. Phase & Time Shift
3. Shaping Filter/Matched Filter
4. Crosscorrelation shallow statics/"Warping": used to interpret time differences
5. Time-Variant Shifts: used to interpret amplitude differences

APPENDIX F: Detailed calculations for the Gassmann calculated time-delay map

To determine the changes expected after fluid injection, calculations are made using the Gassmann equation and the Batzle and Wang (1992) fluid derived properties. The calculations are then converted to time-values and displayed on a map (Figure 27). This map suggests that the Gassmann equation underpredicts the velocity changes. The values used for the calculations are from the reservoir simulation data. Most of the calculations are done within the CMG software. The actual equations entered into the software are in brackets <…>. Note that **2 means to square a term.

1. Find the bulk modulus and the density of water, oil, gas and solvent at each grid point using the Batzle and Wang (1992) fluid derived properties. The parameters used to input into these equations are found in Table F-1. The results of the calculations are shown in Table F-2.

Table F-1. Fluid input values for the Batzle & Wang (1992) calculations

Pressure (MPa)	Temperature (°C)	Gas-Oil-Ratio	Oil Gravity (API)	Gas Gravity	Solvent Gravity
17	87	79.78	39	0.683	1.13

Table F-2. Fluid output values from the Batzle & Wang (1992) calculations

	Water	Oil	Gas	Solvent	Dolomite
Density ρ (g/cm^3)	0.9832	0.7279	0.1272	0.293	2.87
Bulk modulus K (GPa)	2.5005	0.6771	0.0334	0.056	94.9

2. Find the density of the combined fluids. Then find the total density of the rock.

<$Density_{2002\_fluid} = (S_w*\rho_w)+(S_o*\rho_o)+(S_g*\rho_g)+(S_{sol}*\rho_{sol})$>

<$Density_{2002} = (\rho_{dolo} * (1-\varphi))+(Density_{2002\_fluid} * \varphi)$>

3. Find the arithmetic and the harmonic bulk modulus of the fluids. Calculate the average of the arithmetic and the harmonic values. Then find the dry bulk modulus. Then use the Gassmann equation to find the bulk modulus of a saturated rock.

   <$K_{fluid\_harmonic\_2002} = 1/((S_w/K_w)+(S_o/K_o)+(S_g/K_g)+(S_{sol}/K_{sol}))$>

   <$K_{fluid\_arithmetic\_2002} = (S_w*K_w)+(S_o*K_o)+(S_g*K_g)+(S_{sol}*K_{sol})$>

   <$K_{fluid\_average\_2002} = (K_{fluid\_arithmetic\_2002} + K_{fluid\_harmonic\_2002}) / 2$>

   <$K_{dry} = \rho_{dolo} * (1-\varphi) * (V_{P\_dry}**2) / 1.7127 / 1\ 000\ 000\ 000$> Please refer below for details on the K_{dry} calculations.

   <$K_{sat\_2002} = K_{dry} + (((1-K_{dry}/K_{dolo})**2)/((\varphi /K_{fluid\_average\_2002})+((1-\varphi /K_{dolo})-(K_{dry}/K_{dolo}**2)))$> This is the Gassmann equation.

4. Calculate the velocity at each grid point.

$$V_P = \sqrt{\frac{K_{sat} + \frac{4}{3}\left(\frac{K_{sat}}{\left(\frac{V_P}{V_S}\right)^2 - \frac{4}{3}}\right)}{\rho}} \qquad (11)$$

   <$Velocity = SQRT (1.7127 * K_{sat\_2002} * 1\ 000\ 000\ 000 / Density_{2002})$>

5. Knowing the height of each grid block, calculate the travel time where time is the grid thickness divided by the velocity.

   <$Time\_2002 = grid\_thickness / velocity_{2002}$>

6. Do steps 2-5 for both the 1987 data and the 2002 data.

7. Subtract the 1987 travel time from the 2002 travel time to find the time difference. Then multiply by two to account for two-way travel time. <Time_difference = (Time_2002 – Time_1987) * 2>
8. Since we are comparing these results to the time-delay map, we need to add up the time difference found at each map location. Then our calculations can be plotted and observed in map view.

The above calculations were done in the CMG software. The results are exported to Excel. Then, the map is plotted using MATLAB.

How to calculate K_{dry} for each grid block

$$V_{P\_dry} = \sqrt{\frac{K_{dry} + (4/3)\mu_{dry}}{\rho_{dry}}}; \quad (1)$$

$$V_{S\_dry} = \sqrt{\frac{\mu_{dry}}{\rho_{dry}}} \quad (2)$$

To determine K_{dry}, we need to know μ_{dry}. Unfortunately, there are no dipole shear sonic logs in this field. However, the V_P/V_S ratio was measured in the laboratory on cores from well 15-3 and well 15-15 (Appendix H shows the V_P/V_S data). The V_P/V_S ratio is related to μ by rearranging Equations 1 and 2:

$$\frac{V_{P\_dry}}{V_{S\_dry}} = \frac{\sqrt{\frac{K_{dry} + (4/3)\mu_{dry}}{\rho_{dry}}}}{\sqrt{\frac{\mu_{dry}}{\rho_{dry}}}} \tag{3}$$

Solving for μ_{dry} gives:

$$\mu_{dry} = \frac{K_{dry}}{\left(\frac{V_{P\_dry}}{V_{S\_dry}}\right)^2 - \frac{4}{3}} \tag{4}$$

Now equation (1) can be rewritten in terms of the V_P/V_S ratio rather than in terms of μ.

$$V_{P\_dry} = \sqrt{\frac{K_{dry} + \frac{4}{3}\left(\frac{K_{dry}}{\left(\frac{V_{P\_dry}}{V_{S\_dry}}\right)^2 - (4/3)}\right)}{\rho_{dry}}}; \tag{5}$$

$$\rho_{dry} = \rho_{dolo}(1-\varphi) \tag{6}$$

Solve for K_{dry} using the measured laboratory values found in Table F-3. The porosities, φ, from the reservoir simulation results are different for each grid block and so different K_{dry} values are calculated. K_{dry} is approximately 40 GPa in this study.

Table F-3. Rock physics values taken from Core Analysis laboratory measurements of well 15-3 and well 15-15 at 3000 psi.

V_P/V_S ratio for dry rock	1.791818
V_P/V_S ratio for wet rock	2.010727
V_P for dry rock	5252 m/s

APPENDIX G: Useful Equations

Root-mean-square (RMS) = $\sqrt{\frac{\sum_{i=1}^{N} A_i^{\,2}}{N}}$; used for calculating the amplitude change map

Arithmetic mean = $\frac{1}{N}\sum_{i=1}^{N} A_i$; used for calculating the impedance change map

Normalized amplitude change = $A_{norm} = \frac{A_2 - A_1}{(A_2 + A_1)/2}$

API gravity = $\frac{141.5}{specificgravity} - 131.5$

Where the API gravity is a measure of the density of the hydrocarbons.

Specific gravity is the ratio of a given volume of a substance to that of another substance, such as water. There are no units.

For example, the oil density of Rainbow B is 830 kg/m^3 at stock tank conditions and water density is 1000 kg/m^3. So the specific gravity of oil is 0.830.

Gas specific gravity = density gas / density air, where the density of air is 1.239 kg/m^3 at 15.6 °C and atmospheric pressure.

Gas density at normal conditions = Gas density at reservoir conditions * Gas formation volume factor (FVF)

For example, the gas density at reservoir conditions for the Rainbow B is 141 kg/m^3 and the formation volume factor is 0.0060. So the gas density at normal conditions is 0.846 kg/m^3.

APPENDIX H: V_P/V_S ratio determined from Husky Core Analysis

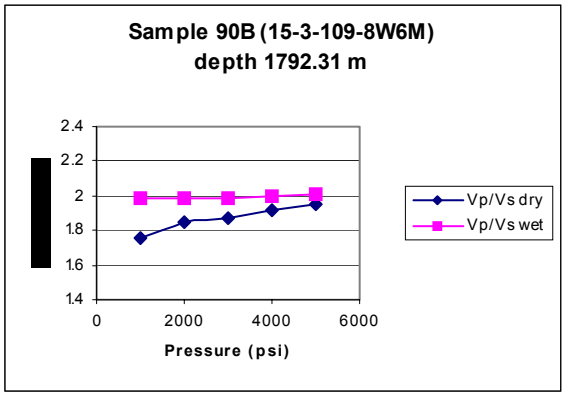

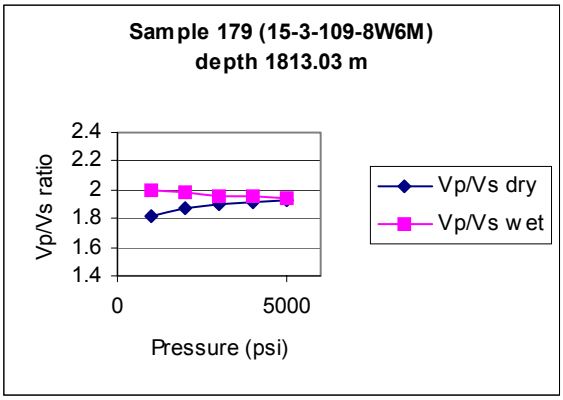

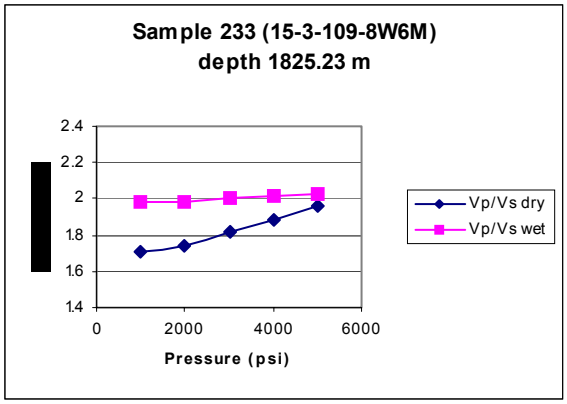

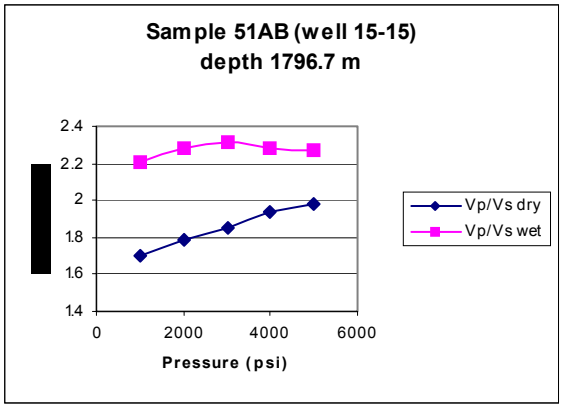

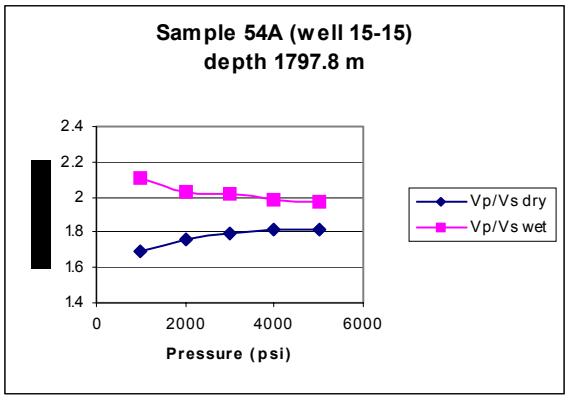

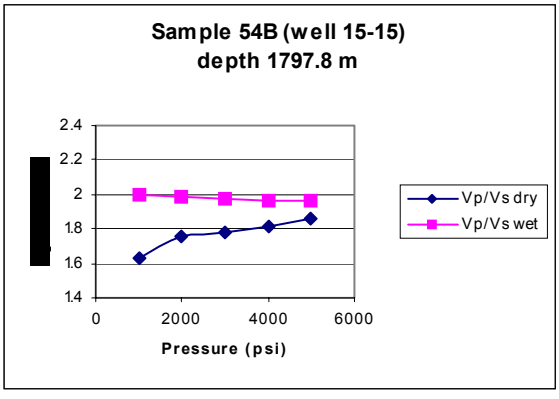

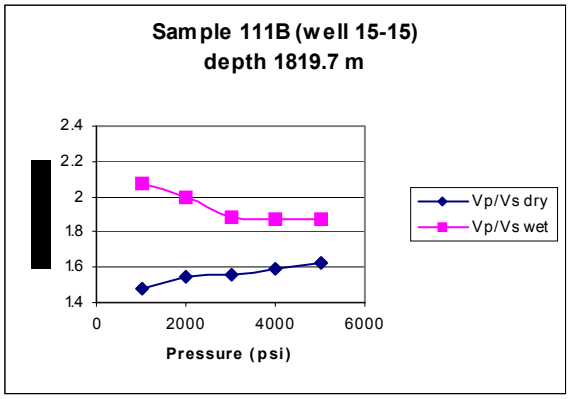
Sample 111B (well 15-15)
depth 1819.7 m
2.4
2.2
2
1.8
1.6
1.4
0
2000
4000
6000
Pressure (psi)
Vp/Vs dry
Vp/Vs wet

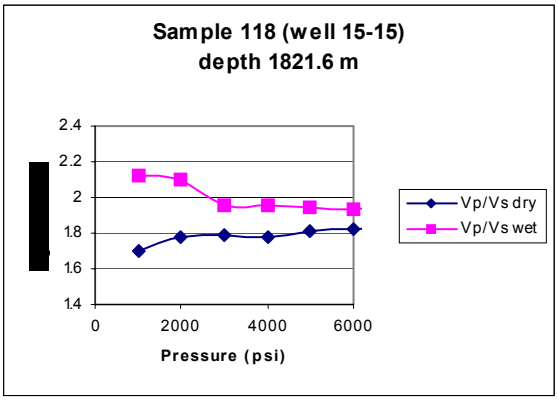
Sample 118 (well 15-15)
depth 1821.6 m
2.4
2.2
2
1.8
1.6
1.4
0
2000
4000
6000
Pressure (psi)
Vp/Vs dry
Vp/Vs wet

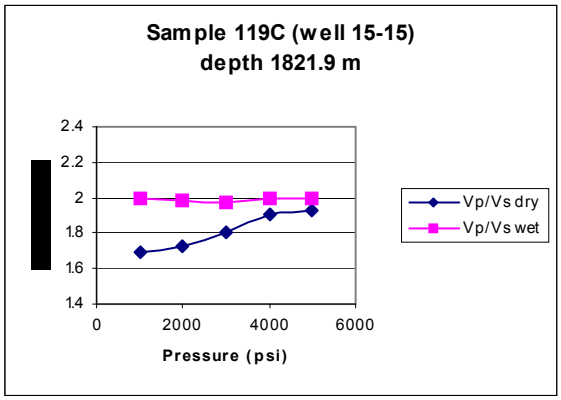
Sample 119C (well 15-15)
depth 1821.9 m
2.4
2.2
2
1.8
1.6
1.4
0
2000
4000
6000
Pressure (psi)
Vp/Vs dry
Vp/Vs wet

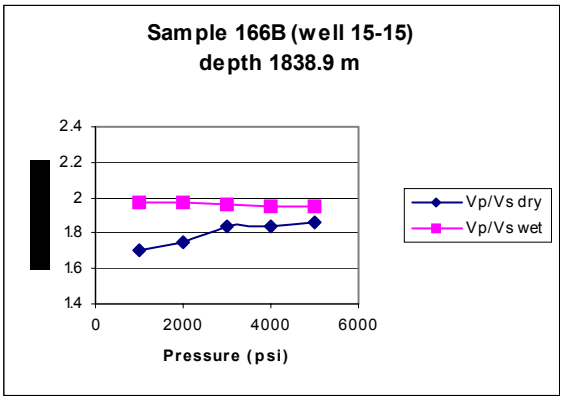
Sample 166B (well 15-15)
depth 1838.9 m
2.4
2.2
2
1.8
1.6
1.4
0
2000
4000
6000
Pressure (psi)
Vp/Vs dry
Vp/Vs wet

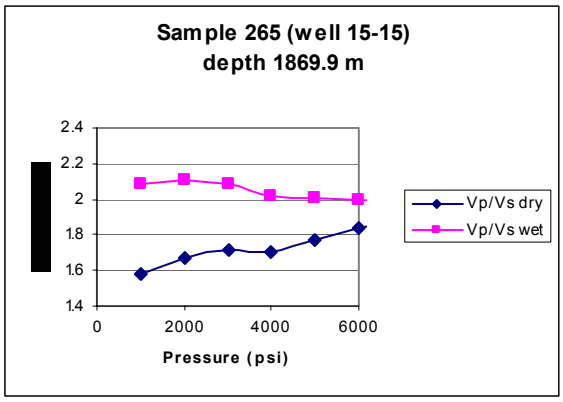
Sample 265 (well 15-15)
depth 1869.9 m
2.4
2.2
2
1.8
1.6
1.4
0
2000
4000
6000
Pressure (psi)
Vp/Vs dry
Vp/Vs wet